USML-1 Glovebox Experiments

Final Report
NASA Contract NAS8-38773

Dr. Robert J. Naumann
Professor of Materials Science
University of Alabama in Huntsville

January 31, 1995

Table of Contents

Figures

Tables

Table of Contents (Appendix)

1.0 Introduction

This report covers the development of and results from three experiments that were flown in the Materials Science Glovebox on USML-1: Marangoni Convection in Closed Containers (MCCC), Double Float Zone (DFZ), and Fiber Pulling in Microgravity (FPM). The Glovebox provided a convenient, low cost method for doing simple "try and see" experiments that could test new concepts or elucidate microgravity phenomena. Since the Glovebox provided essentially one (or possibly two) levels of confinement, many of the stringent verification and test requirements on the experiment apparatus could be relaxed and a streamlined test and verification plan for flight qualification could be implemented. Furthermore, the experiments were contained in their own carrying cases whose external configurations could be identified early in the integration sequence for stowage considerations while delivery of the actual experiment apparatus could be postponed until only a few months before flight. This minimized the time fluids must be contained and reduced the possibility of corrosive reactions that could ruin the experiment. In many respects, this exercise was as much about developing a simpler, cheaper way of doing crew-assisted science as it was about the actual scientific accomplishments of the individual experiments.

The Marangoni Convection in Closed Containers experiment was designed to study the effects of a void space in a simulated Bridgman crystal growth configuration and to determine if surface tension driven convective flows that may result from thermal gradients along any free surfaces could affect the solidification process. This study was motivated by some of the results of the early directional solidification experiments on Skylab in which the ingot was smaller than the ampoule and appeared to have been in only partial contact with the wall. The Soviets observed the similar effects which they attributed to the possibility that the fluid may have been in only partial contact with the wall due to the lack of hydrostatic pressure.

The Fiber Pulling in Microgravity experiment sought to separate the role of gravity drainage from capillarity effects in the break-up of slender cylindrical liquid columns. Both effects tend to limit the parameter range of viscosity and surface tension over which fibers can be successfully drawn. If it can be shown that gravity drainage is a limiting factor in fiber drawing, a good case could be made for using microgravity to draw fibers from lower viscosity melts that are encountered in some of the more exotic heavy metal and fluoride glass systems.

The Stability of a Double Float Zone experiment explored the feasibility of a quasi-containerless process in which a solidifying material is suspended by two liquid bridges of its own melt. This could serve as a simpler method for forming ultra-pure and metastable materials from the melt and can offer a wider variety of configurations for the final product than the various containerless processes that require levitation techniques.

2.0 Background

2.1 Marangoni Convection in Closed Containers

It is generally accepted that Marangoni or surface tension driven convection does not occur in confined solidification experiments because the "no slip" boundaries imposed by the container walls prevent the fluid from moving in response to any interfacial gradient. However, most microgravity solidification experiments have been carried out in partially filled containers in order to allow for thermal expansion and contraction during melting and resolidification. The resulting free surfaces introduce the possibility of Marangoni or surface tension driven convection which could prevent the experiment from achieving diffusion controlled transport conditions that are the objective of most microgravity solidification experiments. Furthermore, many directional solidification experiments have produced ingots that are somewhat smaller in diameter than the container with the appearance that the melt somehow pulled away from the container walls during the solidification process. It is difficult to understand how this comes about, especially in cases where the melt supposedly wets the container walls. Since all such experiments have been done with opaque materials contained in opaque containers that are heated inside furnaces, there has been no way to observe the process, hence we can only speculate on the configuration of the melt during the solidification process and whether or not surface tension driven convection plays a significant role in mass transport during the process. For example, if the vapor space is confined to the end of the melt away from the solidifying interface, as one might expect from minimum surface energy considerations, surface tension gradients across the free surface would be minimal as would be their expected effect on the solidification process. However, the appearance of many solids that have been directionally solidified in low gravity suggests that, in the virtual absence of hydrostatic pressure, the melt may only partially contact the container walls along the axial direction. If this is the case, the "no slip" boundary conditions may not strictly apply and since the thermal and compositonal gradients are strongest in the axial direction, significant surface tension driven convection could result even in closed containers.

2.2 Fiber Pulling in Microgravity

The drawing of thin fibers from glasses and polymers is a well-understood and extremely important technology in our present industrial community. It is generally accepted that in order to successfully draw fibers from a melt, it is necessary for the ratio of the viscosity to surface tension to be greater than a certain value. This is necessary to allow time for the drawn fiber to solidify before it breaks up under the combined effect of Rayleigh instability and gravity drainage. Although optical fibers drawn from silica have virtually revolutionized land line communications technology, they are approaching their theoretical transmissivity which is limited by Rayleigh scattering by the atoms that make up the fiber. Since Rayleigh scattering depends on the inverse fourth power of wavelength, there is much to be gained by operating in the longer wavelength

infrared. This requires making the optical fibers from glass-forming materials that have heavier atoms, such as the fluoride and heavy metal glasses in order to lower the Restralh wavelength. Unfortunately, most candidate materials have viscosity to surface tension ratios in their molten states that are unfavorable to fiber pulling. Thus the ability to extend optical fiber technology into the infrared in order to obtain the potential of ultra-low loss fibers is still an elusive technology.

It has been suggested that microgravity might be able to extend the parameter space over which fibers could be successfully drawn by eliminating the gravity drainage. Of course, there is still the problem of Rayleigh break-up which will be unaffected by gravity. The question to be answered becomes, is there a range of surface tension and viscosity in which gravity drainage is the limiting factor in the ability to draw fibers?

It turned out that the FPM apparatus could easily support a series of experiments proposed by Dr. Dunbar, the Science Commander on this mission, and these were included as part of the FPM experiment. The background for these experiments is described in the following paragraphs.

There are a number of applications where it not possible or feasible to control the position or shape of a melt or other liquid without using physical contact with some solid. When such contact becomes necessary, often it is desirable to minimize such contact by use of non-wetting materials. It may be possible to make surfaces more non-wetting by carefully roughening them. In the virtual absence of hydrostatic pressure, the liquid may just sit on the high points of the rough surface and not penetrate into the valleys.

The degree of wetting is characterized by the contact angle a liquid makes with a surface. This can be measured reasonably well using the sessile drop technique for contact angles less than 90°, however, if the liquid wets the solid poorly, the contact angle will be greater than 90° and it becomes difficult to measure the contact angle because gravity tend to flatten the drop against the surface. In microgravity, the drop virtually free of hydrostatic pressure can relax to its equilibrium shape determined only by interfacial energy and the contact angle can be readily observed and accurately measured. Also, if the hydrostatic pressure really does play a role in the ability of a liquid to wet a surface, the effect could only be seen in a microgravity environment. Finally, if surfaces can be made virtually non-wetting in microgravity, it may be possible to deploy and manipulate droplets passively without physical contact. This may open the possibility for new processing concepts.

2.3 Double Float Zone

One of the attributes of microgravity that has not been effectively utilized in previous space experiments is the ability to deploy novel configurations for processing materials that are either impossible or impractical to achieve on Earth. Obviously, it would be difficult to develop flight experiments based on such concepts since they cannot be tested beforehand on Earth. However, the

use of a glovebox with a Payload Specialist provides a unique opportunity to evaluate the practicality of such concepts using model materials and to answer critical issues such as determining the limits of stability of such configurations in the acceleration environment of a manned space vehicle.

One potentially useful configuration that can only be achieved in reduced gravity is the double floating zone. In practice, a rod or sheet of starting material would initially be heated so as to melt an extended single floating zone, just short of the Rayleigh limit (length = diameter). Then the sources of heat are divided and moved in opposite directions, allowing the molten material in the middle of the zone to cool by radiation to below its solidification temperature resulting in a processed solid that is supported only by two liquid bridges of its own melt. This quasi-containerless process retains all the advantages of containerless processing, except that it is not restricted to small spherical shapes. The much larger surface to volume ratios available allow faster cooling than would be possible with levitated spherical samples, which should aid in glass formation. Also, it should be possible to form the processed material into more useful shapes such as rods, fibers or possibly even sheets.

3.0 Objectives

3.1 Marangoni Convection in Closed Containers

The objective of this experiment was to carry out a fluids experiment in a transparent tube so that the configuration and fluid behavior can be observed during the process. Different fluids were used in two different tubes so that the process can be examined with both wetting and non-wetting conditions. Specific attention was paid to the location of the vapor space relative to the solidification interface and to the nature of the melt-container interface in order to determine if there is complete or partial liquid-solid contact. Marker particles in the form of polystyrene or glass beads were dispersed throughout the fluid to aid in flow visualization to determine if unexpected flows do actually occur. Accelerometer data determined the residual, quasi-steady g-level from which the magnitude of the buoyancy-driven convection can be estimated. However, because of the orientation of the Shuttle during this mission, the buoyancy driven flows were small and nearly perpendicular to the illuminated plane, hence they were not expected to be detectable.

In addition to settling an important issue regarding the flow boundary conditions and the possibility of having unwanted flows in this type of experiment, the data obtained were intoned to provide valuable information on the thermal boundary conditions. Clearly, if there is only partial contact between the melt and the container wall, or between the solidifying material and the container wall, the heat transfer coefficients will be significantly affected, and the careful thermal modeling that has gone into the more advanced solidification experiments being carried out in the Crystal Growth Furnace (CGF) will not be accurate. This experiment can therefore shed some valuable insight into the interpretation of the results from the CGF experiments.

3.2 Fiber Pulling in Microgravity

The objective of the Fiber Pulling Experiment was to determine if there is any benefit to drawing optical fibers in microgravity; more specifically, to see if it is possible to extend the range of parameter space over which fibers can be drawn by going to microgravity. In addition, the time for Rayleigh breakup was measured for various strand diameters for comparison with theory.

A sessile drop experiment that could make use of the FPM apparatus was added at the request of the Dr. Dunbar, the Science Commander for USML-1. The intent was to use of microgravity to enable more accurate measurements of large contact angles and to examine the role of surface roughness and hydrostatic pressure in wetting. Finally, an attempt was made to deploy and position a droplet passively by placing it in a tetrahedral array of small roughened teflon discs.

3.3 Double Float Zone

Clearly one would not want to attempt to utilize a double float zone configuration in an actual process involving high temperature melts making sure that the desired configurations can be achieved and are inherently stable, and until the effects of the residual acceleration of an actual spacecraft are understood. The primary objective of this experiment was an evaluation of the stability of the double floating zone configuration under a variety of circumstances which include length to diameter ratio of the liquid bridge, the ratio of the length of the floating solid to that of the liquid bridges, the shape of the liquid-solid interface, the contact angle between the liquid bridge and the solid, and whether the concept can be extended to sheet configurations. Since the success of the concept requires operating close to the Rayleigh limit for a single zone, for which the critical Bond number (ratio of body force to the surface tension force confining the melt) becomes vanishingly small, periodic residual accelerations (g-jitter) from crew motion and other internal disturbances could be extremely deleterious to the process. Therefore, the secondary objective of the experiment was to evaluate a simple passive vibration isolation concept that may be essential for the practical application of the double float zone technique as well as useful for other experiments, such as protein crystal growth, that are believed to be sensitive to g-jitter.

4.0 Experiment Descriptions

4.1 Marangoni Convection in Closed Containers

The experiment apparatus consists of a control base and a pair of lexan sample tubes. The control base (See Appendix A.1.1.1) contains a simple light sheet illuminator to aid in observing marker particles in the fluid to map the flows. A 5 V Lumitex high intensity bulb is focused on one end of a fiber optic bundle. The opposite end of this bundle is spread into a fan to provide a line source. A 12 mm focal length cylindrical lens projects this line source through the sample

tube . Two metal clips (broom holders from Ace Hardware) hold the sample tube in position over the light sheet illuminator.

The sample tubes were fabricated from 2.54 cm ID lexan tubing (See Appendix A.1.1.2). A copper heater plug in the form of a piston is inserted in one end and a finned copper heat sink plug in the other leaving approximately 3 cm space for the working fluid. The fins unscrew for filling. Double O-ring seals are provided on both the heater and heat sink plug to prevent leakage. These plugs are tightly fit inside the lexan tube, but can move to relieve pressure if necessary. A snap ring on the heater end and a clamp on the heat sink end prevents the plugs from being forced out oh the ends of the lexan tube in the event of an over-pressure situation.

Thermistors are imbedded in both the heater and the heat sink. Thermal control and monitoring of the heater are provided by an Archer (Radio Shack) 277-123 temperature module which controls the power to the heater through a Darlington transistor. A second Archer temperature module monitors the temperature of the heat sink. A thermal fuse in the heater plug protects against overheating in the event of a failure in the thermal control system.

One sample tube was filled with 14 ml Krytox 143AZ leaving approximately a 1 ml void. Krytox 143AZ is a low viscosity fluorocarbon oil. This fluid readily wets the copper plugs as well as the lexan tube. Finding an acceptable non-wetting fluid was not so easy. Water was finally chosen by default even though it is well-known that trace quantities of surface active contaminants, which are virtually impossible to avoid, will tend to suppress Marangoni flow. Lexan, which is initially not wet by water, will after several days absorb a layer of water and become wetted. This happens even with various protective coatings such as Nyebar or 3M FC730. For this reason it was decided to have the crew fill the tube in orbit.

4.2 Fiber Pulling in Microgravity

The fiber pulling apparatus consisted of lexan base and six 3 ml syringes which contained fluids of varying viscosities (See Appendix A.1.2). In addition to the Dow 200 silicone oils that are well-characterized, honey and white corn syrup (Kayro) were also included. This was done because the experiment had been written up as a potential student participation experiment and it was desired to use at least some materials that were familiar and easily accessible to students. Also it was desired to vary the type of materials in order to explore different regions of parameter space.

The fluids and their properties used are listed in Table 1. Fluids A and F are pure 10K cSt and 100K cSt Dow 200 silicone oils. Fluid D is 1 part 100K and 2 parts 10K cSt and Fluid E is 2 parts 100K and one part 10K cSt Dow 200 silicone oil. The viscosities were determined at 22°C by measuring the rate of fall of a 3.2 mm dia. steel BB in a 0.9 mm ID test tube and computing the viscosity from Stokes law. Corrections were made for the additional drag from

the walls of the test tube according to the empirical correction developed by Francis [1]; e.g.

$$\frac{\text{actual viscosity}}{\text{measured viscosity}} = \left(1 - \frac{D_{drop}}{D_{tube}}\right)^{2.5} = 0.335.$$

The surface tensions of the Dow silicone oils were taken from their accompanying data sheets. The surface tensions for the Kayro syrup and honey were measured using the pendant drop technique [2].

Table I. Fluids used in fiber pulling experiment

Fluid	Surface tension	Viscosity
A. Dow 200 Silicone oil	21.5 dynes/cm	11,400 cSt.
B. White corn syrup (Kayro)	62 dynes/cm	7,200 cSt.
C. Beechwood honey	62 dynes/cm	15,000 cSt.
D. Dow 200 Silicone oil	21.5 dynes/cm	45,000 cSt.
E. Dow 200 Silicone oil	21.5 dynes/cm	73,000 cSt.
F. Dow 200 Silicone oil	21.5 dynes/cm	100,000 cSt.

It should also be pointed out that the mechanism for forming liquid strings in normal gravity is quite different than in low-gravity in that gravity drainage is helping pull the liquid into a strand. In low-gravity, attempts to pull liquid strings by simply dipping a object into the fluid and removing it were unsuccessful as was discovered during the KC-135 training flights prior to this mission. Without the help of gravity drainage, the viscous forces are not strong enough to overcome the inertia of the liquid and the string immediately breaks. In order to deploy a liquid strand , it is necessary to extrude the liquid as the syringe is moved to avoid having to accelerate the liquid in the strand.

A syringe containing the fluid of choice was selected and inserted through a guide hole in the experiment base. A small amount of fluid was squeezed onto a pedestal supported by the base to anchor the liquid strand. The syringe was then slowly withdrawn while extruding fluid in an attempt to form a thin liquid strand approximately 5 cm long. The syringe was then clamped in place and the breakup of the column was recorded on video. Of interest was the time required for the capillary instability to cause the column to thin and separate as a function of column diameter, viscosity and surface tension.

The teflon discs for the Sessile Drop experiment were prepared at Worcester Technical University under the direction of Dr. Al Sacco, the backup Mission Specialist. Varying degrees of surface roughness were obtained by scoring

groves into the surface of the discs. Each disc was drilled and threaded on its backside to accept a screw from a 1 cm dia. lexan rod that could be clamped into FPM base. Crew water was used for the sessile drop experiment. Red food coloring (Kroger brand) and liquid detergent (Johnson's baby shampoo) was carried in syringes to support this experiment.

The Passive Drop Positioning experiment utilized an Al frame in which 4 1 cm dia. teflon discs were mounted in a tetrahedral configuration such that their faces were tangent to a 2.54 cm dia. sphere at the center. The surfaces of these discs were roughened by scoring. Crew water, colored with the red food coloring was used to form the drop to be positioned.

4.3 Double Float Zone

The apparatus consisted of a lexan base with two clamps to hold two 1 cm dia. lexan support rods along a common axis (See Appendix 1.3). The clamps allow the distance between the rods to be easily adjusted. One set of lexan support rods is flat on one end and rounded on the other end. A small hole bored along the axis of the end pieces accommodates a teflon sleeve which encases the alignment wires to prevent the working fluid (water) from wicking back into the hole as the alignment wire is withdrawn. The end faces of the rods were coated with EHEC CST103, a sucrose-like coating to improve the wettability of the lexan. Teflon shrink tube was placed over the cylindrical surfaces to act as an anti-spread barrier.

A second set of end pieces are similar lexan rods that have a flat plate on one end whose edge is perpendicular to the axis in order to support a sheet of liquid rather than a cylindrical column. These end pieces also have a small hole bored along the axis to accommodate a teflon sleeve which encases the alignment wires. Two stainless steel alignment wires are stored in the experiment container along with the end pieces and the float pieces.

The float pieces consist of two short lexan rods, one with flat ends and one with round ends; two long lexan rods, one with flat ends and one with round ends; and a small flat lexan plate. Small holes drilled a short distance at each end of the float pieces accommodate the alignment wire to aid in the setup and deployment of the liquid bridges. The wetted surfaces of the float pieces are also coated with EHEC CST103 and teflon shrink tube was place over the lateral surfaces to prevent unwanted spreading.

The Mission Specialist positions the float piece between the support rods by engaging the alignment wire into dimples on each face of the float piece. The rods are adjusted to leave a gap of approximately 1 cm between the float piece and the support rod on each side. These gaps are filled with water using a syringe. The alignment wires are then slowly withdrawn leaving the float piece suspended by the two liquid bridges. The bridges are extended by pulling the alignment wires farther apart and adding more water until the configuration becomes unstable and breaks up. The procedure is recorded on video. The details of the planned experiment sequence are in Appendix A.2.3.

The vibration isolator consists of a frame containing the suspension and caging mechanism and an isolation plate fabricated from a magnetic mild steel (See Appendix A.1.4). The base of the double float zone experiment attaches to this plate during operation by means of magnetic strips glued to its bottom with Epon 812 epoxy.

An elastomeric mechanism suspends the isolation plate within the channels of the frame. This mechanism should be critically damped and should have a resonant frequency less than 1 Hz.

Since the suspension system must have an extremely high compliance to provide the low resonant frequency desired, a caging mechanism was required to support the weight of the isolation plate during launch and during the setup operations in the glove box. The caging mechanism consisting of four grooved stainless steel discs with one flat side. When these discs are rotated such that the grove engages the isolation plate, they provide rigid support of the experiment until the crew member is ready to evaluate the isolation concept. The Payload Specialist can uncage the isolation plate from within the glovebox with a minimum of disturbance to the isolated portion of the experiment by rotating these discs until their flat surface faces the isolation plate. To recage the isolation plate when the experiment is completed, the discs are rotated back until the grooves re-engage the isolation plate.

5.0 Experimental Observations

5.1 Marangoni Convection in Closed Containers

Sample tube #1 was filled with water on orbit with no difficulty leaving a 1 ml void or bubble as requested. Marker particles were injected, and the sample tube was closed. The heat-up was nominal with the heater temperature stabilizing at 45°C as programmed. The heat sink temperature gradually rose from ambient (25°C) to approximately 30°C during the course of the experiment as predicted, verifying that the thermal gradient was established throughout the sample. Initially the bubble was located on the tube wall near the heat sink and showed no tendency to move. By mechanically jiggling the tube, the Mission Specialist was able to reposition the bubble near the hot end where the thermal gradient was steeper. The Mission Specialist reported no evidence of marker particle motion. This was not unexpected since, as mentioned previously, any trace of surface active contaminant will prevent Marangoni convection in water.

The primary purpose of this run was to examine the configuration of a fluid in an ampoule in which the ends were wetted (simulating the interaction between a melt and a forming solid) and the walls were highly nonwetting. It was speculated that under these circumstances there might be a tendency for the fluid to pull away from the walls because of the very large contact angle between the water and the Nyebar-coated lexan walls. However, the bubble appeared nearly hemispherical in shape and tended to remain pinned to the wall at one spot with significant contact line resistance.

After these initial observations, plans called for the experiment to be placed out of the way in the back of the Glovebox and monitored by video to see if disturbances from vernier thruster firings could be detected and analyzed. Since the fluid had a known temperature gradient and was free of Marangoni effects, this would have been a good opportunity to analyze the effects of transient accelerations on fluids in partially filled containers, a topic of interest to experimenter who carry out solidification experiments in containers with void space to allow for thermal expansion. Unfortunately, this portion of the experiment apparently did not get recorded.

Sample tube #2 containing Krytox 143AZ represents a system in which the fluid wetted both the walls and the ends. Again, at the beginning of the heating cycle, the bubble was located at the heat sink end near the wall. However, this time the bubble was perfectly spherical and did not actually touch the wall. Approximately 2-3 minutes after the heater was turned on, the heater temperature stabilizing at 45°C as programmed. Because of the lower thermal conductivity of the Krytox oil and shorter duration, the heat sink temperature remained at ambient (25°C) during the course of the experiment. At 504 sec after the heater had been turned on, the bubble began migrating toward the heated end, slowly at first but accelerating rapidly as the bubble moved into warmer liquid where the viscosity was lower and the temperature gradient was steeper. However, after reaching the heater plug, instead of remaining near the center of the tube, the bubble migrated to the wall opposite the light source. Several times the Mission Specialist mechanically jiggled the apparatus in an attempt to move the bubble back to near the center of the sample tube, and each time the bubble migrated back to the same side. This direction is nearly perpendicular to the residual gravity vector. Also when the Mission Specialist later turned the apparatus 180°, the bubble migrated in the opposite direction to the same wall. Therefore, this could not be a buoyancy effect from the residual gravity. (Estimated bubble rise in 1 micro-g is 0.0007 cm/sec.) It should be noted that on each attempt to re-center the bubble, the bubble never actually crossed the center line of the apparatus which could account for the fact that migration was always to the same wall.

Considerable motion of the marker particles in the fluid was also observed after the bubble came to rest against the heater plug and the side of the sample tube. The flow was clearly being driven by the thermal gradient across the bubble, as would be expected. The flow direction appeared to be across the heater face to the bubble, around the face of the bubble in the direction of the negative thermal gradient, then along the wall toward the heat sink, and eventually circulating through the chamber back to the heater face. The bubble essentially acts as a pump which drives a circulating fluid flow throughout the sample tube.

5.2 Fiber Pulling in Microgravity

Attempts to pull long slender liquid strands were made using all 6 sample materials. Strands of liquid were successfully pulled from all of the silicone oils, including the 10,000 cSt. material which does not tend form liquid strings in

normal gravity. Their time for break-up ranged from several seconds to more than a minute for higher viscosity silicone oils. However, it proved difficult to pull liquid strands from the aqueous polymer systems (corn syrup and honey) which easily form strings in unit gravity. Their time to break-up due to capillarity effects was at most a second or so, presumably because of their higher surface tension.

To deploy a uniform liquid strand requires a steady translation motion synchronized with the plunger motion. This proved to be a difficult task manually, exacerbated by the tendency of the syringe to stick in the guide hole. The high viscosity liquid strands tended to snake around as they were being deployed. Also, surface tension tended to pull the fluid away from the nozzle of the syringe and back to the pedestal as the strand was being deployed. Consequently, most of the strands were of not of uniform diameter, a factor not accounted for in the theory of liquid strand breakup.

The procedure called for several attempts to draw strands a different pull rates to vary the diameter. Since only one syringe was provided for each fluid, this was attempted by sucking the fluid back into the syringe and redeploying the strand. Generally, the first attempt was the most successful because it was difficult to avoid incorporating air bubbles as the fluid was drawn back into the syringe. In retrospect, it would have been better to have used individual syringes to repeat the experiments at different pull rates.

The sessile drops were deployed as planned. Initially, the drops tended to wet the teflon discs more than had been observed in previous KC-135 flights. This was apparently due to contamination on the surface of the discs even though they had been cleaned with a detergent in an ultrasonic bath and rinsed with DI water followed by an isopropyl alcohol rinse prior to their pre-flight stowage. These were recleaned on-orbit and the experiment rerun with better results. Contact angles approaching 180° for the most severely roughened surfaces were observed and photographed. (The detailed analysis and reporting of this experiment is the responsibility of Dr. Dunbar.)

A liquid drop was successfully deployed and positioned in the Passive Drop Positioning experiment with the drop just barely touching the roughened teflon discs. However, when a small drop of liquid detergent was added, the drop immediately wet the discs and was lost.

5.3 Double Float Zone

A single liquid bridge was established at or near the Rayleigh limit and observed using the vibration isolator in both the caged and uncaged position. When uncaged, the isolator worked quite well; the looped rubber band suspension system supplying sufficient restoring force to keep the floating platform near the center of the apparatus. However, the spacecraft environment was sufficiently quiet so that vibrations of the liquid column were not seen either with the platform caged or uncaged. The Mission Specialist displaced the experiment several times from its equilibrium position and it slowly returned with

only a slight overshoot and a period of approximately 1 sec. Therefore, the system appeared to be well damped with a natural frequency on the order of 1 Hz. The Mission Specialist reported that a slight bias was present, probably caused by unequal tension in the rubber band suspension system.

Because the vibration level in the Glovebox was so low that disturbances in the liquid bridge were not apparent, and in the interest of time (several other Glovebox experiments exceeded their allotted time), it was decided to not use the vibration isolator for the remainder of the DFZ experiments.

Double float zones of various lengths were established using the flat ended support rods with the short, flat ended float rod. These configurations were remarkably stable even when they were intentionally perturbed by the Mission Specialist. A curious and unexpected phenomena was observed, however. The floating rod seemed to be more attracted to one support rod that the other. Adding more fluid to the short zone seemed to exacerbate the effect. In fact, at one point the short zone was bulging while the long zone was pinched in - totally defying all expected behavior! It was demonstrated this was not a residual gravity effect since the residual g-vector was perpendicular to the direction of offset and turning the apparatus around produced the same effect.

When this result was reported at an IAF meeting shortly after the USML-1 mission [3], Prof. Dieter Langbein (University of Bremen) pointed out that this behavior was a consequence of the Young-Laplace equation which states that the pressure in the liquid zone is proportional to the net curvature of the liquid surface. The net curvature is the sum of the reciprocals of the two principal radii. A short bulging zone could have the same net curvature as a long pinched-in zone; the larger contribution from the shorter principal radius being compensated for by the negative curvature of the larger principal radius. He has since analyzed this problem and has shown a point at which two cylindrical zones bifurcate into an unduloid (bulging out) and a nodoid (pinched in) figures of revolution.

A sheet and a double sheet float zone was also established. From the limited video down-link available during this period, it did appear that a stable sheet of considerable length could be established although there was considerable bulging in the center, as would be expected. The flat float piece was captured and held by the two flat liquid bridges, but it tended to cock or rotate approximately 20° in the plane of the sheet. This appeared to be caused by unequal wetting along the faces of the support rids and the flat float piece.

Lack of time limited the number of runs scheduled with the other double float zone configurations. The long rod with flat ends appeared to behave very much like the shorter rod except, because of the larger mass, the oscillation frequency when perturbed was much lower. The support rods were turned around and double float zones were established with the rounded wetted interfaces. These did not appear to be as stable as with the flat end rods. This may have been due to the fact that the water did not seem to wet the rounded ends as well.

Time did not permit extension of the system to near the Rayleigh limit or to establish the limits of stability.

6.0 Analysis of Results

6.1 Marangoni Convection in Closed Containers

6.1.1 Analysis of the Bubble Motion

After the bubble first started to move, the position of the mid point of the bubble was determined at various times by averaging the top and bottom locations and the left and right side locations using the image processing software. The velocity was determined for a point representing the average of two successive positions by dividing their difference by the elapsed time. The results are shown in Fig. 1.

The weighted average thermal diffusivity of the Krytox oil and the lexan tube was calculated to be $\kappa = 0.000643$ cm^2/sec. The thermal time constant, $L^2/\kappa = O(10^5)$ sec; therefore the system is far from steady state. The temperature distribution in the fluid is estimated by solving the one-dimensional time dependent heat flow equation with the end walls held at constant temperatures. This solution can be written as

$$T(y,t) = T_{cold} + (T_{hot} - T_{cold})\left[(1 - y/L) - \frac{2}{\pi}\sum_n \frac{1}{n}\sin(n\pi y/L)\exp\left(-\kappa n^2\pi^2 t/L^2\right)\right]. \quad (1)$$

A theory for the motion of a bubble in a thermal gradient was developed by Young, Goldstein, and Block (YGB) [4] whose result can be written (after correcting typographical errors in the original paper as pointed out by Szymczyk [5])

$$\vec{v} = -\left(\frac{2}{3\mu(2\mu + 3\mu')}\right)\left[\frac{3\mu R}{(2 + h'/h)}\left(\frac{\partial\gamma}{\partial T}\right)\nabla T + (\rho - \rho')(\mu - \mu')\vec{g}R^2\right] \quad (2)$$

where R is the droplet radius, μ is the absolute viscosity, and h is the thermal conductivity. Unprimed quantities refer to the host fluid and primed to the fluid in the droplet. For an air bubble in a liquid in 0 gravity, this simplifies to

$$\vec{v} = -\frac{R}{2\mu}\left(\frac{\partial\gamma}{\partial T}\right)\nabla T. \quad (3)$$

For Krytox oil, $\partial\gamma/\partial T = -0.07$ dynes/cm and at 45°C, $\mu = 12$ cSt. Therefore, for R = 0.425 cm and $\partial T/\partial x = O(10°C/cm)$, v = O(1 cm/sec) which is an order of magnitude larger than the highest observed velocity. However, it should be

remembered that since the YGB theory assumes creeping flow and neglects convective heat transport, it is valid only in the limit of vanishing Marangoni number, $Mg = \left|(\partial\gamma/\partial T)\nabla T\right| R^2(\mu\kappa)^{-1}$. For a bubble with R = 0.425 cm, the Mg = O(3000) and the thermal Peclet number, $v R / \kappa$ = O(100). Therefore, thermal convection cannot be neglected and its effect would be to reduce the thermal gradient around the droplet which would lower the driving force. Also, the YGB analysis assumes the droplet to be in an infinite medium; whereas in our application, wall effects would also have to be considered since the diameter of the bubble is not small compared to the diameter of the tube. This effect could lower the bubble velocity in this experiment by a factor of at least 3. [1]

Therefore, to model the droplet motion, the YGB equation is multiplied by some correction factor K to account for the lowering of the thermal gradient by thermal convection and for the additional drag from the walls. The temperature and thermal gradient were computed for each observed position of the bubble at the time of the observation. Since μ is a function of temperature, an empirical fit of the form $\mu(T) = 104.7\ \exp(-0.04816\ T)$ for 20°C < T < 45°C was used. The K-value at each point was obtained by dividing the observed velocity by the YGB equation. An average K-value was then found and used to plot the trajectory shown in Fig. 1.

Initially, each observed time was taken to be the time after the heater was turned on. This produced the dotted line in Fig. 1, which does not quite fit the data. Also, the resulting individual K-values were found to increase from ~0.6 at the cold end to ~0.9 at the hot end. Since a finite time is required for the heater to come up to temperature after it is turned on, an adjustment should be made for this fact. A much better fit was obtained (solid line in Fig. 1) by subtracting an empirically determined effective warm-up time of 73 sec from each observed time. The average K-value from this fit was 0.09 and the individually determined K-values were more consistent over the range of observations. Fig. 2 shows the thermal profile predicted by the model at the start and end of the bubble motion.

6.1.2. Global flow

Selected particles were mapped over an extended time using the video analyzer to obtain the streamlines for the global flow. These are illustrated in Fig. 3.

The global flow was modeled numerically by solving the linearized steady state Navier-Stokes equations for the stream function Ψ in two-dimensions,

$$\frac{\partial^4\psi}{\partial x^4} + 2\frac{\partial^2\psi}{\partial x^2}\frac{\partial^2\psi}{\partial y^2} + \frac{\partial^4\psi}{\partial y^4} = 0\,. \qquad (4)$$

A 21 by 21 grid was used with the bubble represented by an octagon in one corner. Boundary conditions were $\Psi = 0$ at all edges including the bubble, and

$\Psi' = 0$ at all edges except the free side of the bubble perpendicular to the heater plug. Here the Ψ' was set to the velocity of the surface tension driven flow. Convergence was obtained using a simple relaxation method. The resulting streamlines are shown in Fig. 3 which are seen to be in qualitative agreement with the particle tracks in Fig. 4.

The computed horizontal velocity at the middle of the chamber (halfway between the right and left walls) is shown in Fig. 5. Similarly, Fig. 6 shows the computed vertical velocity midway between the hot and cold ends. These velocities are normalized by the maximum velocity at the bubble surface which was observed to be 0.107 cm/sec. Measured normalized velocities from particle tracks crossing these lines are shown for comparison. The agreement is seen to be reasonably good on a global scale even though the model is relatively coarse and neglects the variation of viscosity with temperature. The major discrepancy is the failure of the model to account for the higher velocities of the particles near the heater surface as they are being drawn into the region near the bubble. This is due to the lack of resolution in the grid. However, since the primary function of the model is to relate the Marangoni flows driven by the bubble to the global flow, the coarse resolution and simplifying assumption of a constant viscosity seem to be adequate for this purpose.

6.1.3 Estimated buoyancy-driven convection

In the vicinity of the Glovebox in the Spacelab module, the quasi-steady residual acceleration was approximately 1 micro-g. The buoyancy-driven flow from this acceleration can be estimated from Batchelor's approximate solution to the equation for the stream function in a rectangular cavity with a linear thermal gradient for low Rayleigh numbers (which he attributes to Grashof) [6]. The maximum velocity for the case of a square can be written as

$$v = \frac{Gr}{144\sqrt{3}} \frac{\nu}{L} . \qquad (5)$$

The thermal expansion coefficient for Krytox oil is 6.1×10^{-4}. Taking L = 2.54 cm, DT = 20°C, and an average value for n = 19.44 cSt/r =0.194/1.86 = 0.104 cm^2/sec, the $Gr = (980 \times 10^{-6})\ (20)(6.1 \times 10^{-4})(2.54)^3/(0.104)^2 = 0.0181$. From this, the maximum velocity from buoyancy-driven convection is 3×10^{-6} cm/sec which is 3 orders of magnitude less than the global velocity driven by Marangoni convection for the case in question.

6.1.4 Analysis of the bubble drift to the wall

Post flight testing revealed no measurable thermal asymmetry across the heater plug. Of course on earth the fluid configuration is quite different than in low gravity. In the vertical thermally stable position (hot over cold) the bubble is flattened across the heater because of hydrostatic pressure and Marangoni convection is suppressed because of the stabilizing thermal gradient. In any

other position, the heat transfer is significantly affected by buoyancy-driven convection.

Since the Krytox oil has a low thermal conductivity and the Marangoni convection was relatively large in the vicinity of the heater, heat transfer is dominated by the convective transport. Therefore, cold fluid is being brought to the heater plug by the flow and becomes heated as it flows along the heater face. If the bubble were exactly centered, the configuration would be unstable because any slight displacement would allow the fluid that traveled the greatest distance along the face to become hotter, thus reducing the interfacial energy on that face of the bubble. Apparently, equilibrium is reached only when the bubble moves all the way to the wall where the fluid flowing in from the side has traveled the greatest distance along the heater face and has reached the highest temperature before encountering the bubble. One could argue that this effect should produce the opposite result; i.e., the radial thermal gradient would be from the wall toward the center, hence the migration should be in the direction of the thermal gradient which would drive the bubble back to the center. On the other hand, the flow along the hotter side nearer the center would be stronger than on the side nearer the wall which could produce a rolling motion along the heater face which could carry the bubble to the wall. Unfortunately, the lighting on the wall side of the bubble was shadowed by the bubble, and no definitive flow data could be obtained on this side of the bubble. Therefore, the cause of this unexpected effect cannot be conclusively resolved.

6.2 Fiber Pulling in Microgravity

In 1892 Lord Rayleigh obtained a solution for the break-up of slender liquid columns, both for the inertial dominated case and for the viscous dominated case [7]. The time constant for the latter is given by

$$\tau = \frac{6\mu a}{\sigma} \tag{6}$$

The video frames showing the liquid strands were captured just after deployment and analyzed to obtain the strand length, and the maximum and minimum diameter of the strand. The observed breakup times for the various liquid strand were obtained from the clock superimposed on the frames. These data are presented in Table 2 along with the τ computed from eq. 6.

Since the liquid strands were not cylindrical, some decision had to be made about which radius should go into eq. 6 for comparison. Since the observed mode of breakup always started from the thinnest part, it was decided to use the minimum radius.

It was determined from measurements of known objects in the video frame (the diameter of the pedestal and the diameter of the syringe tip) that 35 pixels on the video camera were equivalent to 1 cm. Therefore, the measurement resolution was essentially 1 pixel or 0.03 cm. However, the relative error could be quite large, especially for the strands that only measured a few pixels in

diameter. The limits of accuracy imposed by this constraint are indicated in Table 2 as the max. and min. values for τ. Also, the breakup times could only be resolved to the nearest second, so this relative error could be quite large for liquid strands with short life times.

Nevertheless, the data computed from Lord Raleigh's model is in reasonable agreement with the observed breakup time, considering that τ is actually a time constant during which the strand thins by 1/e, and does not correspond to the actual time of fracture of the liquid strand. The resolution of the video image was not good enough to measure the rate at which the strand thins.

The major anomalies seem to be with the data from fluids D and E. The first attempt with fluid D had what appeared to be a small bubble at the syringe tip in the final deployed configuration which probably caused premature breakage. It is not clear why the subsequent runs did not persist longer. It can only be speculated that they also may have contained unseen bubbles that limited their lifetime.

In the case of fluid E, the recorder was turned on after the only strand was deployed. Therefore, there is no way of knowing the breakup time other than to say it is greater than the observed time. Actually, it is not even known if this was the first and only deployment, or the last deployment)

6.3 Double Float Zone

The resolution of the video images of the liquid zones was not sufficient to obtain the actual zone shape. Therefore, the data was analyzed by approximating the shape of the zones by circular segments fitted to the end points at the rods and to the midpoint. From the geometry shown in Figure 7, the following relationships are obtained.

The radius of curvature is obtained from the measurement of L and h by the relationship

$$(R-h)^2+(L/2)^2 = R^2 \tag{7}$$

from which

$$R = \frac{L^2}{8h}+\frac{h}{2} \tag{8}$$

The pressure inside the liquid zone is given by the Young-Laplace equation,

$$P = \gamma\left(\frac{1}{R}+\frac{1}{r_0+h}\right). \tag{9}$$

The force on the disc at the end of the liquid zone is

$$F = \pi r_0^2 \gamma \left(\frac{1}{R} + \frac{1}{r_0 + h} \right) - 2\pi r_0 \gamma \cos\theta \qquad (10)$$

and $\cos\theta = (R-h)/R$.

The radius of the zone as a function of z is given by $r(z) = r_0 + h - \delta(z)$ where $\delta(z) = R\left(1 - \sqrt{1 - z^2/R^2}\right)$. The volume of the liquid zone is obtained from

$$V = \pi \int_{-L/2}^{L/2} r(z)^2 \, dz. \qquad (11)$$

The length and diameter data presented in the Table 3 is in the units of pixels obtained directly from the video analyzer. The r_0 for the left hand (LH) side was taken to be 21.25 pixels while, because of a slight camera parallax, the RH side was found to be 20.4. These numbers are averages taken from all of the frames that were analyzed. There was no evidence that the apparatus or camera was moved significantly during the experiment, but the rod diameter readings from the individual frames did vary by as much as from 41 to 45 on the LH rod and from 39 to 44 on the RH rod. The differences are attributed to the difficulty in locating the rod surface because of the low contrast on the video image. Similar difficulties were encountered in measuring the liquid zone length and diameter. The ±1 error limits shown in the data reflect the least count of the measurement. The actual measurement may be in greater error because of the above mentioned difficulties. Those measurements with fraction values are averages of measurements from several frames in which the state of the system remained the same. In some cases, only a few frames were available before the state of the system was changed and here the measurements were taken from a single frame.

The calculated force data were normalized by the force on a cylindrical zone which is given by

$$F = \pi r_0^2 \gamma \left(\frac{1}{r_0} \right) - 2\pi r_0 \gamma = -\pi r_0 \gamma \qquad (12)$$

and the computed volume data is normalized by the volume of a cylindrical zone having the initial zone length, 34.4 pixels for the LH zone and 33.2 pixels for the RH zone. To give an estimate of the sensitivity of these computations, the upper figure represents the maximum value within the bounds of the indicated error, the lower figure is the minimum value, and the center is the middle figure is the value computed from the stated data.

7.0 Conclusions

7.1 Marangoni Convection in Closed Containers

A model for the observed bubble migration in the time-dependent temperature field was developed that requires the bubble to move 11.1 times slower than predicted by the YGB theory. This is believed to be due to wall effects since the bubble to sample tube diameter is not negligible, and to convective thermal transport around the bubble which is not considered in the YGB formulation.

The mechanism causing the bubble to migrate to the wall of the sample tube is not understood. Since the walls of the sample tube have a higher thermal conductivity than the Krytox oil, they may have been slightly hotter before the steady state temperature field was reached. This would produce a radial thermal gradient that would drive the bubble toward the wall. Another possibility is that, if the bubble is slightly off-center, there will be stronger flow toward the bubble from the side of greatest distance from the wall since there is less viscous damping in this region. The unequal pressure from turning these flows as they near the bubble would continue to drive the bubble away from the center and toward the wall.

Marangoni convection around the bubble in a thermal gradient can act as a pump to circulate fluid throughout the volume. The resulting flows are seen to be global in nature with velocities ranging from 2-5% of velocity at the bubble surface, which for the present experiment was ~ 0.1 cm/sec. While flows of this magnitude may be inconsequential relative to natural convection in normal gravity, they are several orders of magnitude larger than the buoyancy-driven flows in typical microgravity experiments. Even though the most intense flow is concentrated in the hot end of the sample tube away from what would be the solidification interface, there was sufficient global flow that could certainly affect heat or mass transport in such experiments.

Experimenters should be aware that such flows are possible even in closed containers if there are any free surfaces in the form of void spaces or gas bubbles in the presence of either a thermal or solutal gradient.

A manuscript describing this experiment has been accepted for publication in Journal of Crystal Growth.

7.2 Fiber Pulling in Microgravity

The observed time required for a long slender column of silicone oil to break up is in reasonable agreement with the prediction from the theory developed in 1892 by Lord Rayleigh for Newtonian fluids, even though the actual fluids used are probably non-Newtonian. This is probably the first attempt to actually test of this theory since there is really no way to perform such a test on Earth without gravity interfering. It was difficult to get an accurate measure of the initial diameter of the liquid column since there was some variation in diameter due to

the manual deployment technique used. Also, there is some uncertainty in when the time should start since it takes several seconds to deploy the strand, during which some thinning has already begun. Greater accuracy could probably be obtained with a mechanical deployment system which could meter the fluid more accurately than by hand.

It is interesting to note that in the case of honey and corn syrup, the break-up time was so short because of the higher surface tension that it was difficult to draw strands in microgravity, whereas they readily form long liquid strings in unit gravity. Apparently gravity drainage helps stabilize these strands against break-up due to capillarity effects by continuing to supply new fluid to areas that have begun to thin. Conversely, it was possible to draw strings of the lower surface tension 10K cSt silicone oil in microgravity which does not string in normal gravity, presumably because of the rapid gravity drainage permitted by the lower viscosity. Therefore, it would appear that the only region of parameter space in fiber drawing that might benefit from microgravity would be that of low viscosity, low surface tension. However, it is also interesting that the 10 K cSt silicone oil has a higher viscosity than the corn syrup yet the corn syrup has more tendency to form strings on earth. This difference is most probably due to different rheological properties giving further evidenced that the problem is more complex than Lord Raleigh's analysis would indicate.

The feasibility of controlling the position of liquid drops with minimal contact was demonstrated by use of small, textured non-wetting plates arranged in a tetrahedral (or higher symmetry) pattern around the drop. One restriction is that the drop must remain approximately the size that will just fit inside the array, thus the technique may not be applicable to systems that evaporate or otherwise change size appreciably. On the other hand, this scheme may be useful for minimizing contamination during solidification of a molten drop.

A manuscript describing this experiment is in preparation for submission to J. Spacecraft and Rockets.

7.3 Double Float Zone

Double float zones in a variety of configurations were deployed and appeared to be quite stable for $L/D < 2.7$ in one of the zones. An unanticipated asymmetry between the two zones was observed which appears to be explained by a bifurcation in the force balance diagram as predicted by Langbein. An attempt was made to analyze the observed data by approximating the shapes of the liquids in the two zones using circular segments in order to obtain the net curvature required by the Young-Laplace equation. The agreement was only fair and it is not clear whether the discrepancy is due to the error in the approximation, or in the inability to measure accurately the zone shape from the video data. The low contrast of the video data made it very difficult to precisely locate the surface of the zone. A more precise analysis of these data is being undertaken by Langbein in which the observed data will be fit by unduloids which represent the actual solution to the Young-Laplace equation. This work will be submitted as a joint publication to Microgravity Science and Technology.

7.4 General Conclusions

The Glovebox has proven itself as an excellent facility to do small, relatively simple, crew assisted experiments. The ability to interact with the crew during the course of the experiments was especially helpful, particularly when unexpected results were observed. This means the experiments should be performed during times of real-time down-link whenever possible and the video data recorded directly. It was found to be generally unsatisfactory to rely on the on-board recorded data since one has no way of knowing the quality of the data, or even if the right data was being recorded.

The only real problem encountered in the analysis of this set of experiments was the lighting which resulted in poor contrast in parts of the video image. This made it difficult to digitize some of the data. Perhaps more attention should have been paid in trying to optimize the experiment placement and background during the training sessions, but some aspects of the experiment could not be performed on earth and there is only a limited amount of flexibility within the confines of the Glovebox. Future experimenters, who plan to utilize video data, would do well to design their own lighting scheme into the experiment, as was done in the MCCC experiment.

8.0 References

1. A. W. Francis Physics 4 (1933) 403-406
2. S. Fordham, J. Fluid Mech 194 (1948) 1-15
3. R. J. Naumann, "Preliminary Results from Three USML-1 Glovebox Experiments", paper IAF-92-0902, 43rd Congress of the International Astronautical Federation, Washington, DC, Aug. 1992
4. N. O. Young, J. S. Goldstein, and M. J. Block, J. Fluid Mech. 6 (1959) 124.
5. J. A. Szymczyk, Appl. Microgravity Tech. II (1989) 49
6. G. K. Batchelor, Quarterly Appl. Math. XII (1954) 209.
7. Lord Rayleigh, Phil. Mag. S. 5., 34 (1892) 145-155

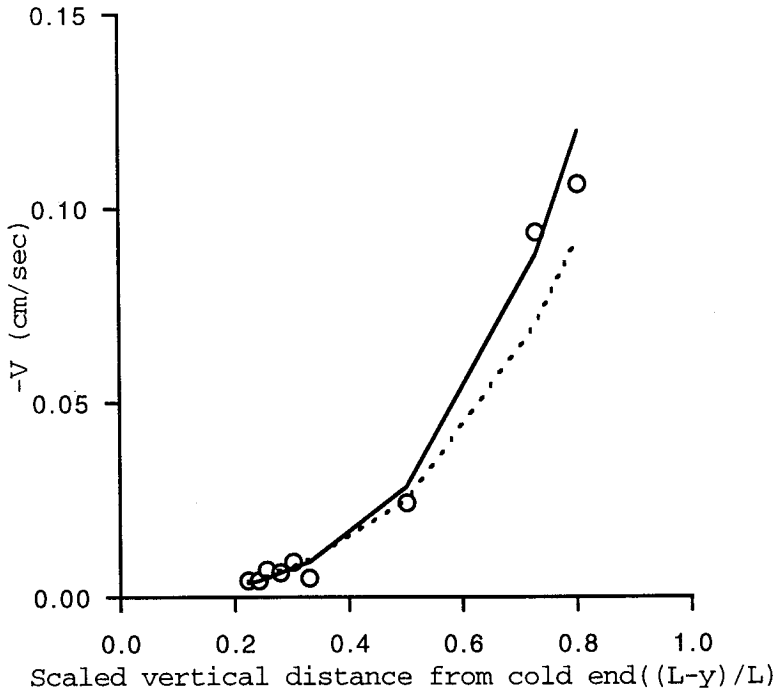

Fig. 1. Observed bubble velocity as a function of position along the chamber axis (circles). The dashed line represents the modeled bubble velocity taking the observed time as the time after heater turn-on. The solid line represents the modeled bubble velocity after subtracting 73 sec from the time the heater was turned on to account for warm-up.

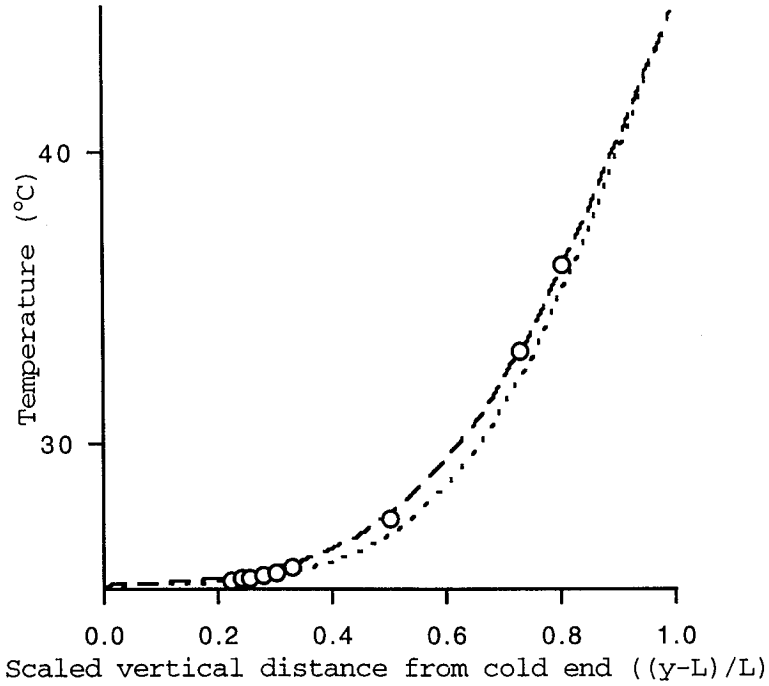

Fig. 2. Modeled thermal profile when bubble motion started (dotted line) and when ended (dashed line). Circles represent the temperature at each observed point.

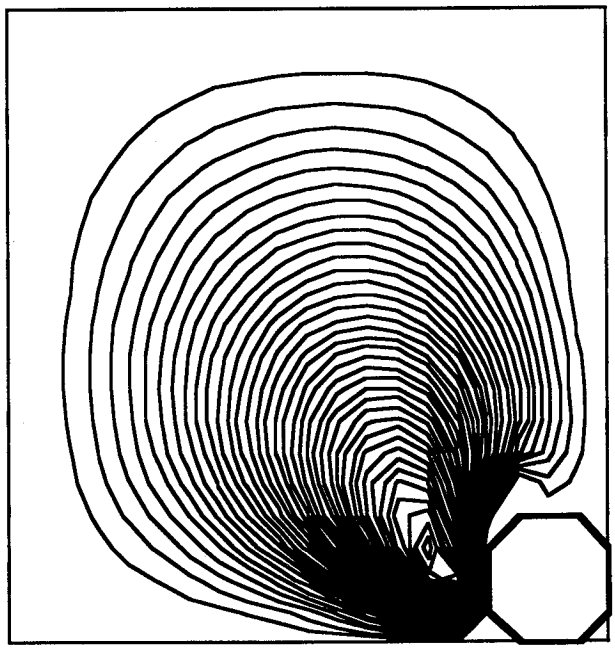

Fig. 3. Stream function computed from the numerical model. The heater is along the bottom edge of the diagram and the heat sink is at the top edge. Flow is along the bottom edge, up the vertical surface of the bubble (represented as the octagon in the lower right hand corner), and around the chamber in the right hand sense.

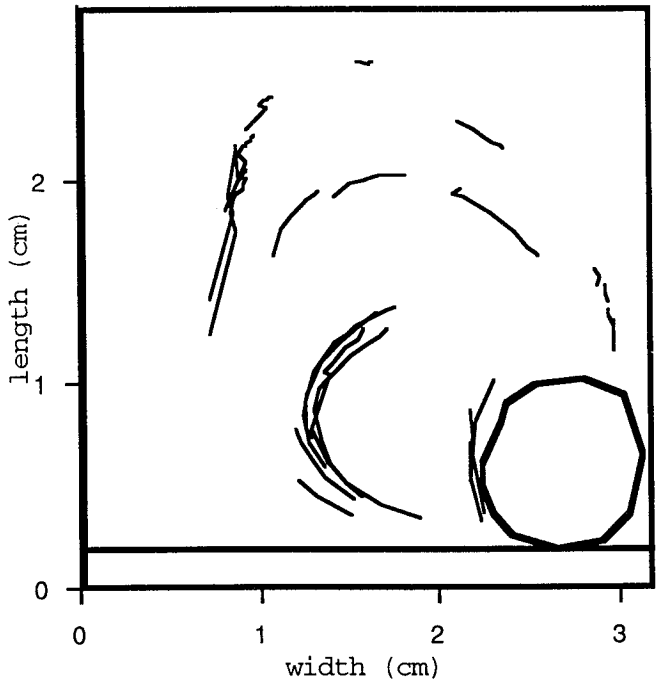

Fig. 4 Observed particle trajectories which map out the streamlines in the experiment. These are seen to be reasonably with the computed stream function in Fig. 3. The heater is the second horizontal line just above the origin. This is slightly different from the bottom that the reference system was based on because of parallax in the video camera view.

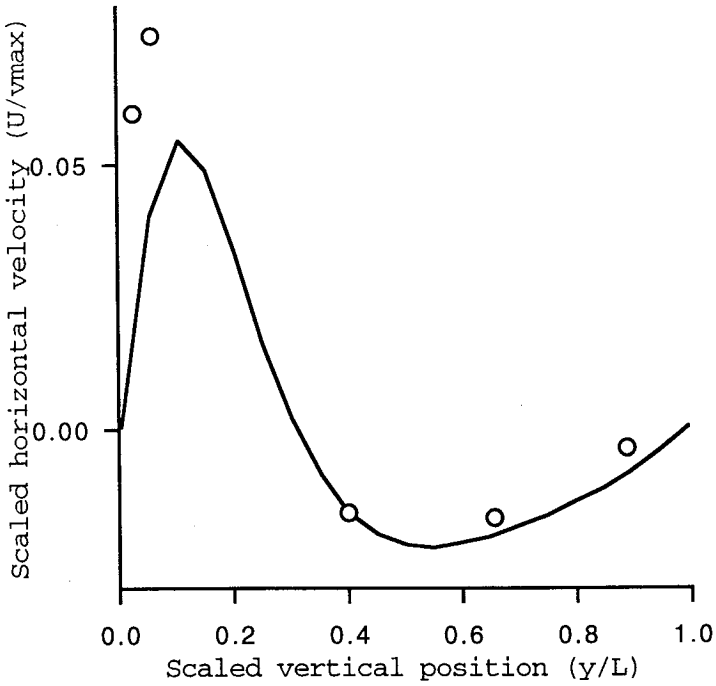

Fig. 5. Horizontal velocity scaled by the maximum velocity at the bubble taken midway between the side walls. The solid line is from the numerical model. The circles represent measured data points.

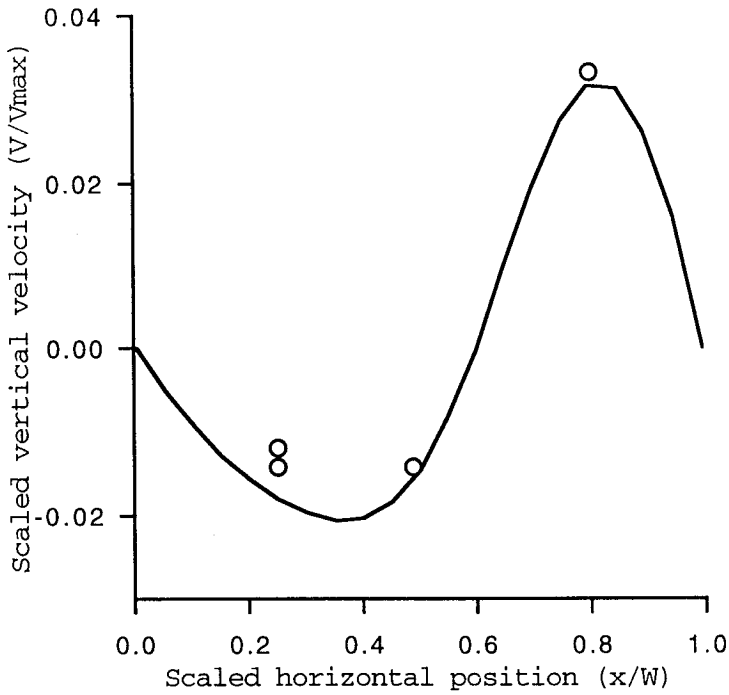

Fig. 6. Vertical velocity scaled by the maximum velocity at the bubble taken midway between the heater and the heat sink. The solid line is from the numerical model. The circles represent measured data points.

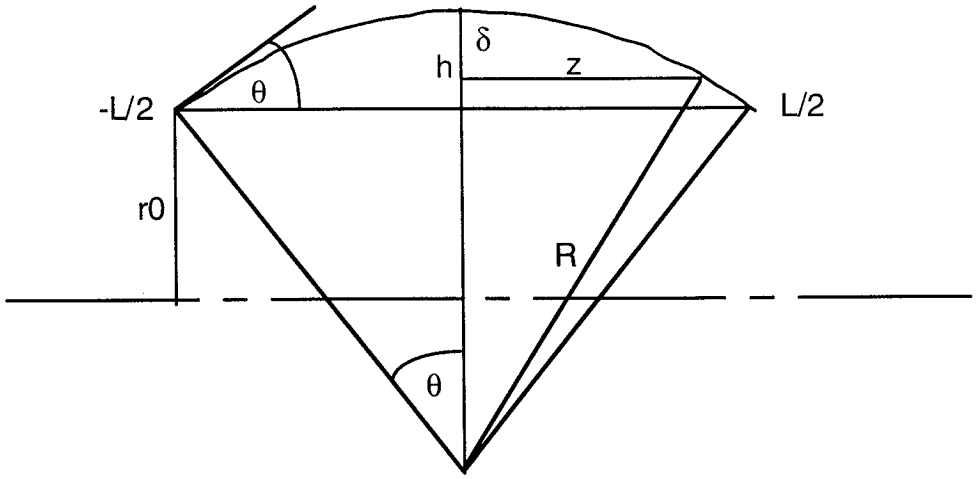

Figure 7. Geometry used for calculation of pressure in the liquid zones.

Table 2

Fluid	Length	Max Dia	Min Dia	Lifetime	Tau	Tau max	Tau min	
A	2.57	0.34	0.31	9 sec	5.24	5.72	4.77	
A	3.69	0.46	0.26	8 sec	4.29	4.77	3.81	
B	3.20	0.46	0.20	2 sec	0.70	0.80	0.60	
C	2.00	0.43	0.23	4 sec	1.67	1.88	1.46	
C	4.51	0.51	0.26	2 sec	1.88	2.09	1.67	
D	3.09	0.57	0.29	13 sec	18.82	20.70	16.93	had bubble at small end
D	3.06	0.11	0.06	2 sec	3.76	5.64	1.88	
D	3.66	0.69	0.20	8 sec	13.17	15.05	11.29	
E	4.14	0.31	0.14	>21 sec	15.22	18.26	12.18	deployment not recorded
F	3.86	0.37	0.23	63 sec	33.45	37.63	29.27	

DFZ data

Time	L (LH)	Dia (LH)	F (LH)	V (LH)	L (RH)	Dia (RH)	F (RH)	V (RH)	F'(RH)	V'(RH
			0.56	1.30			0.41	1.42	0.54	1.33
18:03:40	34.4±1	50.2±1	0.44	1.26	33.2±1	50±1	0.27	1.33	0.41	1.26
			0.34	1.19			0.11	1.25	0.26	1.18
18:04:10	Separated rods									
			1.00	1.17			0.91	1.27	0.98	1.20
18:05:36	48.75±1	36±1	0.98	1.15	36±1	44±1	0.84	1.20	0.93	1.14
			0.96	1.08			0.78	1.13	0.86	1.07
18:03:07	Added fluid to LH									
			1.00	1.60			0.96	1.25	1.02	1.18
18:05:50	50±1	44±1	0.98	1.59	36.5±1	43±1	0.90	1.18	0.98	1.12
			0.96	1.45			0.84	1.11	0.93	1.05
18:05:52	Added fluid to RH									
			0.95	1.51			0.84	1.66	0.90	1.57
18:06:02	47±1	46±1	0.92	1.43	43±1	47±1	0.78	1.58	0.85	1.49
			0.89	1.36			0.71	1.49	0.79	1.41
18:06:08	Separated rods									
			1.01	1.57			0.87	1.62	0.92	1.52
18:06:52	54.33±1	40.67±1	1.00	1.49	42.67±1	46.33±1	0.81	1.53	0.87	1.45
			1.00	1.42			0.76	1.45	0.82	1.37
18:07:27	Removed fluid from LH									
			0.93	1.38			0.86	1.52	0.92	1.43
18:07:59	57±1	34.5±1	0.90	1.31	40.5±1	46±1	0.79	1.44	0.87	1.36
			0.86	1.24			0.74	1.36	0.80	1.29
18:08:34	Separated rods									
			0.75	1.22			0.75	1.44	0.84	1.35
18:08:57	61±1	30±1	0.70	1.16	37±1	47±1	0.66	1.36	0.76	1.28
			0.64	1.09			0.59	1.28	0.67	1.21
18:09:19	Separatred rods									
			0.68	1.27			0.80	1.55	0.87	1.46
19:09:36	66±14	29±1	0.63	1.20	40±1	47±1	0.73	1.47	0.81	1.38

			0.57	1.14			0.65	1.39	0.74	1.31
18:09:50	Moved LH rod closer									
			0.96	1.36			0.81	1.47	0.88	1.39
18:09:50	41±1	45±1	0.92	1.29	38.5±1	46.5±1	0.73	1.39	0.82	1.31
			0.86	1.22			0.64	1.31	0.74	1.24
18:10:13	Moved rods closer									
			0.51	1.39			0.44	1.45	0.56	1.36
18:10:15	35±1	51±1	0.39	1.31	34±1	50±1	0.31	1.37	0.44	1.29
			0.25	1.24			0.15	1.29	0.30	1.21
18:10:43	Added fluid to RH									
			0.43	1.42			0.40	1.54	0.51	1.44
18:10:46	35±1	52±1	0.29	1.35	35±1	51±1	0.26	1.45	0.39	1.36
			0.15	1.28			0.11	1.37	0.25	1.29
18:10:48	Separated rods and extracted fluid from RH									
			0.98	1.46			0.87	1.14	0.97	1.07
18:11:17	57±1	37±1	0.96	1.39	32±1	44±1	0.78	1.07	0.90	1.01
			0.93	1.32			0.67	1.00	0.81	0.95
18:11:25	Moved RH rod closer									
			0.86	1.46			0.67	1.14	0.81	1.07
18:11:45	43±1	48±1	0.80	1.39	30±1	46±1	0.54	1.01	0.70	1.01
			0.73	1.32			0.38	1.00	0.56	0.93
18:12:09	Added fluid to RH and separated rods									
			0.87	1.36			0.78	1.32	0.87	1.24
18:12:36	61±1	33±1	0.83	1.29	35±1	46±1	0.69	1.24	0.80	1.17
			0.79	1.22			0.58	1.17	0.70	1.11
18:12:43	Added fluid to LH									
			1.00	2.14			0.81	1.39	0.89	1.31
18:13:03	65±1	45±1	0.99	2.04	37±1	46±1	0.73	1.31	0.83	1.24
			0.99	1.95			0.64	1.24	0.74	1.17
18:13:15	Added fluid to RH and LH and separated rods									

			1.00	2.26			0.89	2.02	0.93	1.91
18:14:13	78±1	41±1	0.98	2.16	51±1	48±1	0.85	1.99	0.89	1.82
			0.97	2.07			0.80	1.83	0.85	1.73
18:15:00	Added fluid to LH and RH and separated rods									
			0.88	2.80			0.93	2.22	0.95	2.09
18:17:42	114±1	36±1	0.85	2.68	56±1	48±1	0.90	2.11	0.93	1.99
			0.82	2.57			0.86	2.17	0.90	1.90
18:17:53	LH zone broke during attempt to add fluid to LH									

USML-1 Glovebox Experiments (Appendix)

Final Report
NASA Contract NAS8-38773

Dr. Robert J. Naumann
Professor of Materials Science
University of Alabama in Huntsville

January 31, 1995

A.1.0 Drawings

A.1.1.1 MCCC Control Base Assembly

REVISIONS				
ZONE	REV	DESCRIPTION	DATE	APPROVED

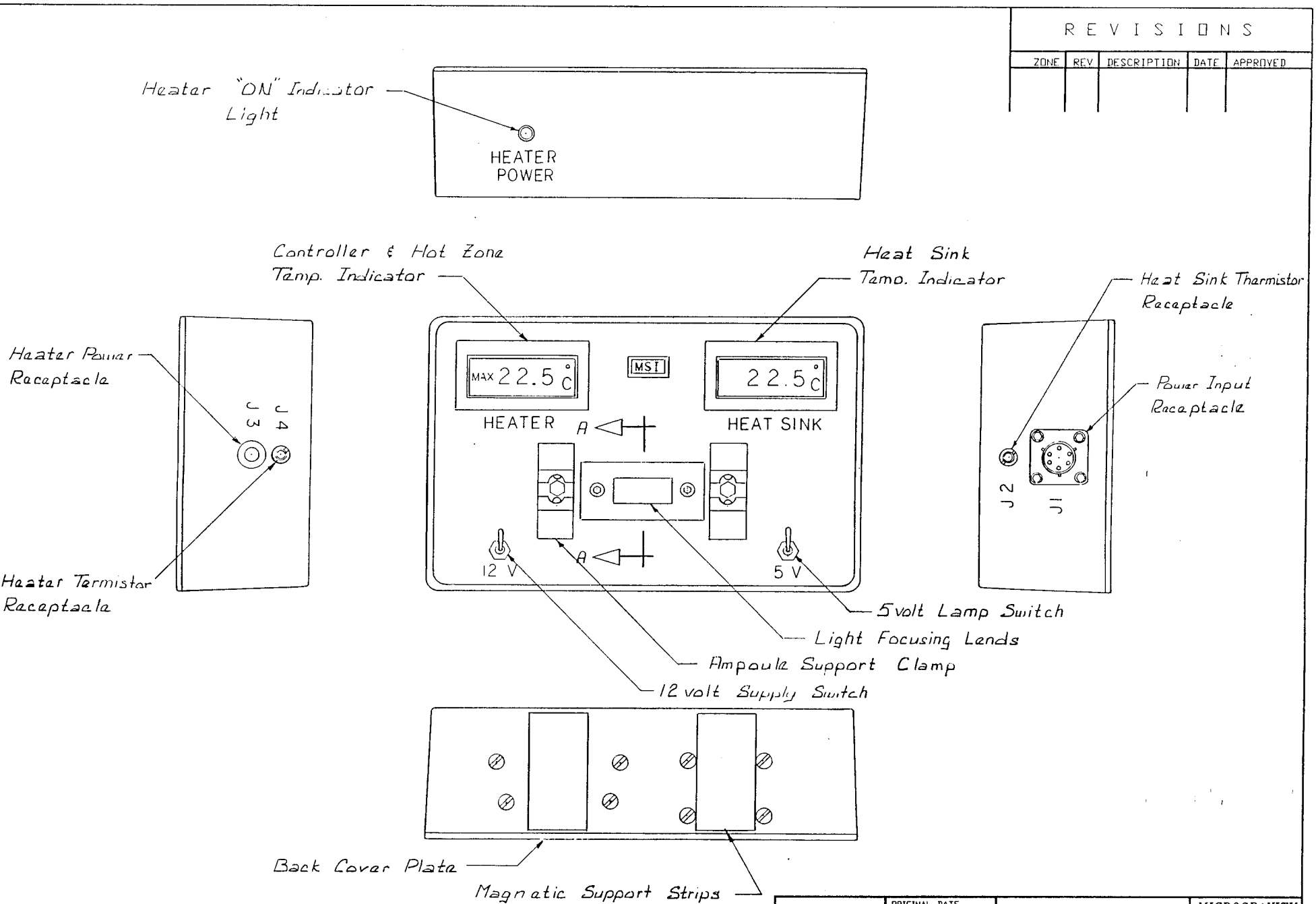

FINISH:	ORIGINAL DATE OF DRAWING 10-11-91	Control Housing Layout	MICROGRAVITY SYSTEMS, INC. HUNTSVILLE, ALABAMA
TOLLERANCE UNLESS NOTED	DRAFTSMAN / CHECKER / ENGINEER / SUBMITTED / APPROVED RDR	WEIGHT / DATE / CODE	DWG SIZE C — DRAWING NUMBER MS-98016

A.1.1.2 MCCC Furnace Assembly

REVISIONS

ZONE	REV	DESCRIPTION	DATE	APPROVED

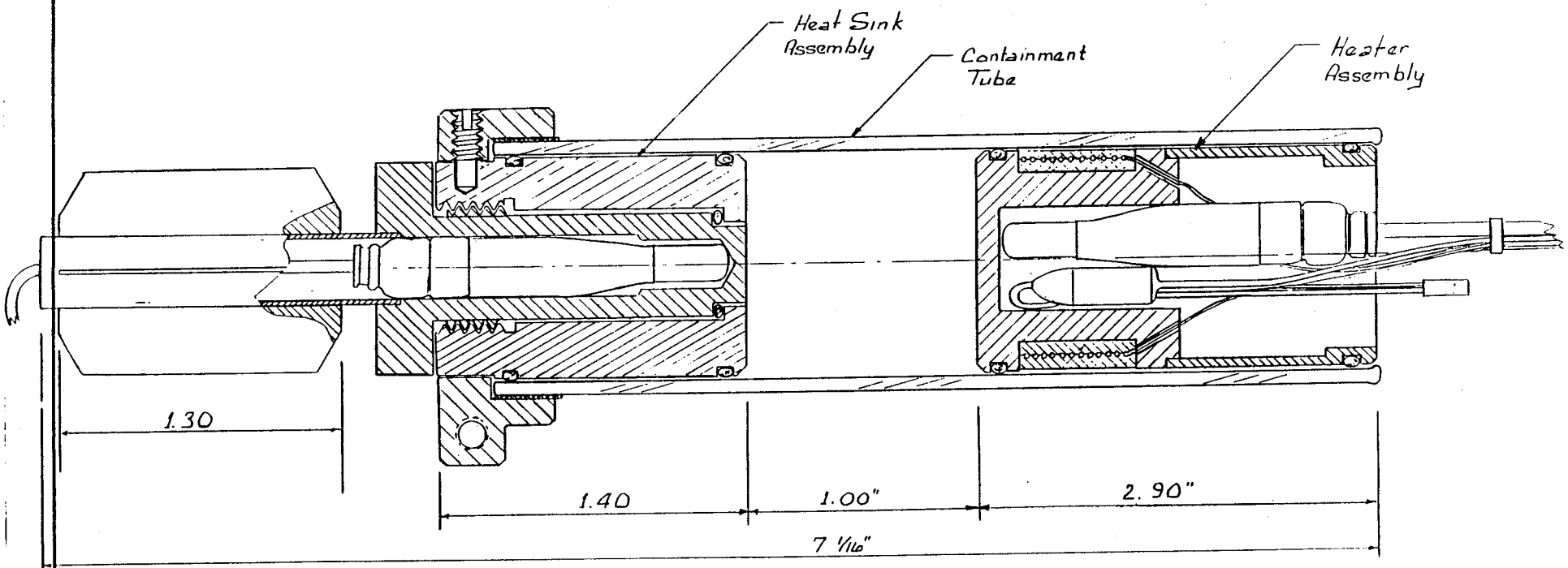

FINISH:	ORIGINAL DATE OF DRAWING 8-14-91	GEM 05 Exp. Furnace Assembly	MICROGRAVITY SYSTEMS, INC. HUNTSVILLE, ALABAMA
TOLLERANCE UNLESS NOTED	DRAWN / CHECKED / ENGINEER / MANAGER		SIZE: B/G; DRAWING NUMBER: MS-98001
	SUBMITTED	NEXT ASSY / DATE / CODE	SHEET: 1 OF 1
	APPROVED BAL	SCALE: / UNIT WEIGHT	

A.1.2 FPM Assembly

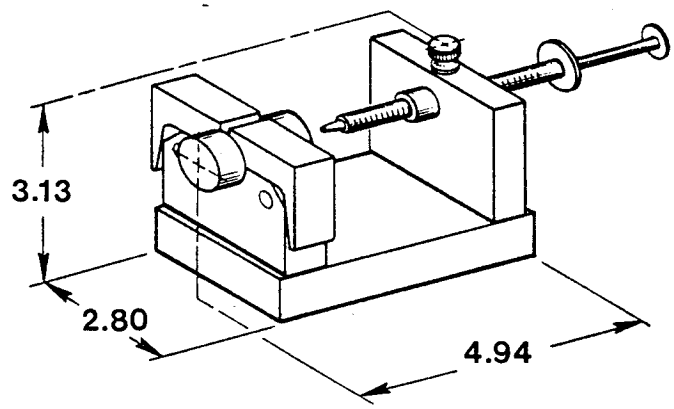

Short Base w/ Flat-Faced Dumb bell and 3 ml syringe

EXPERIMENT #9

FIBER PULLING IN MICROGRAVITY
P/N 90C1670

A.1.3 DFZ Assembly

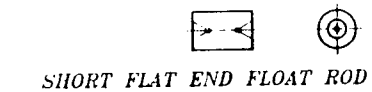

SHORT FLAT END FLOAT ROD

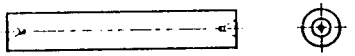

LONG FLAT END FLOAT ROD

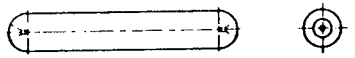

LONG ROUNDED END FLOAT ROD

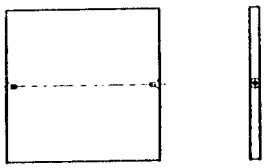

FLAT FLOAT PLATE

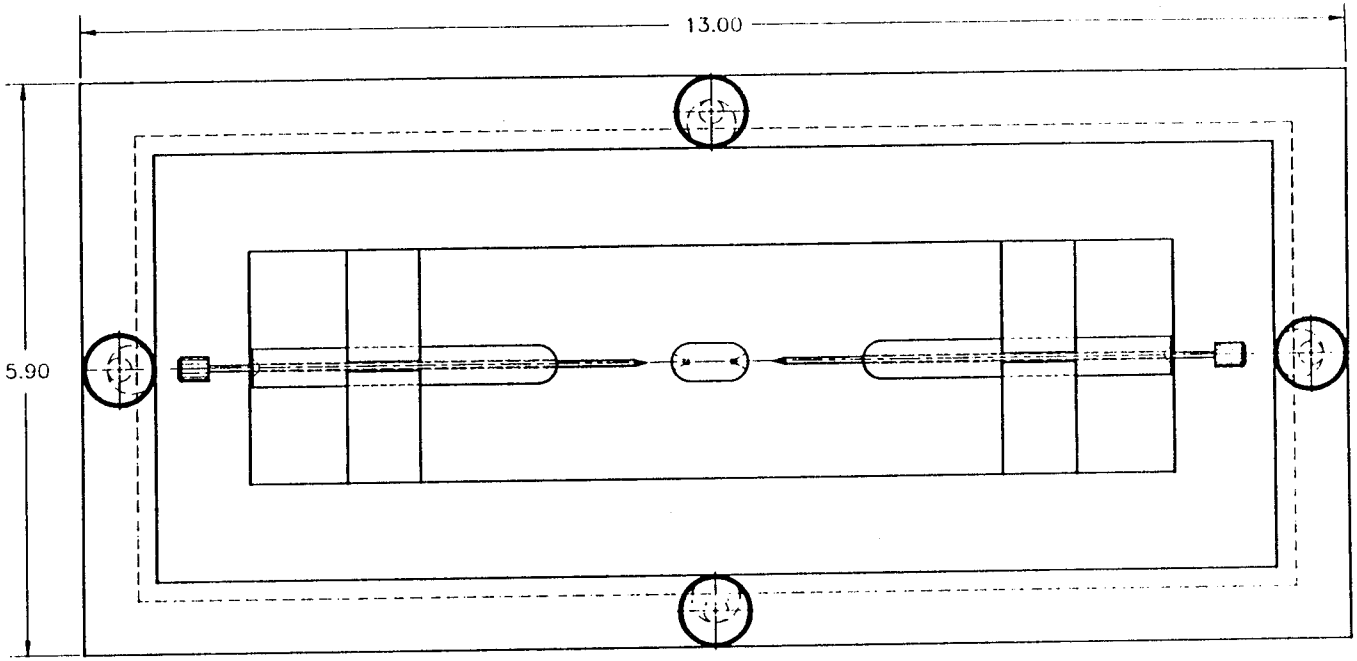

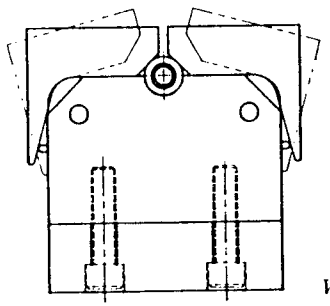

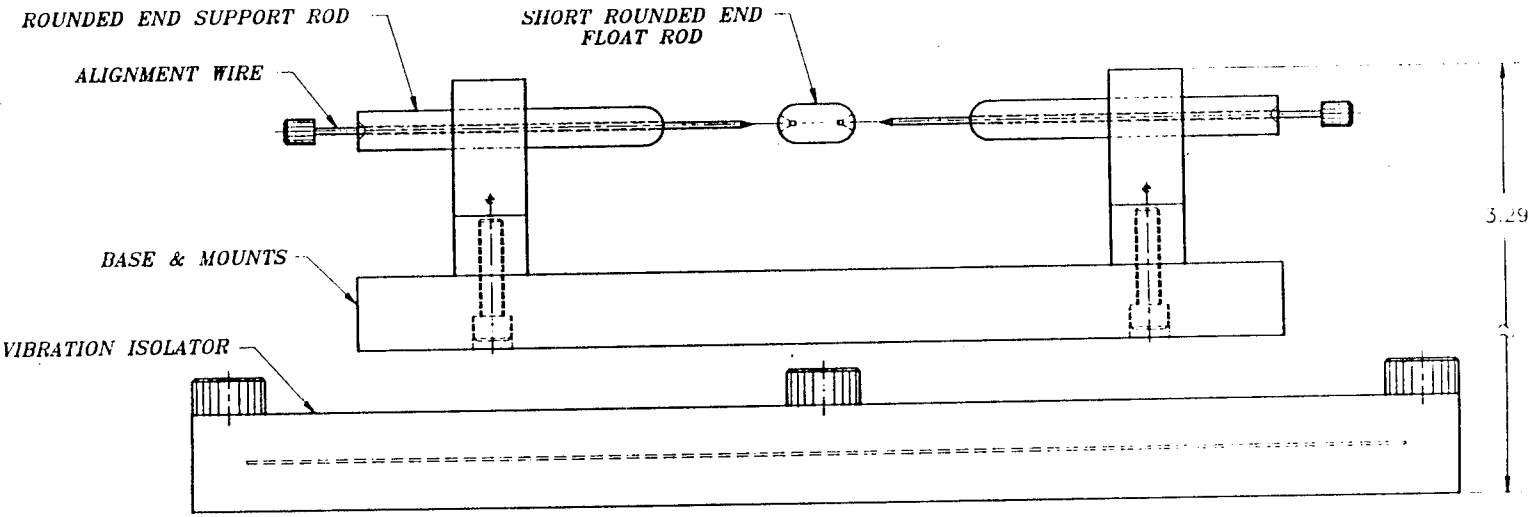

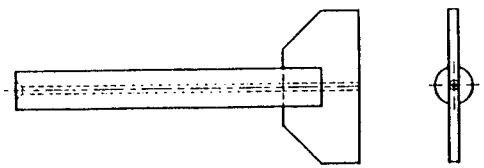

PLATE END SUPPORT ROD

UNLESS OTHERWISE SPECIFIED DIMENSIONS ARE IN INCHES
TOLERANCES ARE:
FRACTIONS ± DECIMALS .XX± .XXX± ANGLES ± °
MATERIAL –
DO NOT SCALE DRAWING

EXPERIMENT NO. 12

STABILITY OF A DOUBLE FLOAT ZONE

SIZE	CAGE NO.	DWG. NO.
C		90C1671
SCALE: 1/1		SHEET 1 of 1

A.1.4 Vibration Isolation Assembly

ORIGINAL PAGE IS OF POOR QUALITY

REVISION				
ZONE	REV	DESCRIPTION	DATE	APPROVED
	A	REVISED DWG. TO SHOW CHANGES ON DETAILED PARTS, & ADDED NOTE 3	7-10-91	
	B	INCORPORATED CHANGES TO DETAIL PARTS. ADDED ITEM NO.'S 12 THRU 15.	10-28-91	

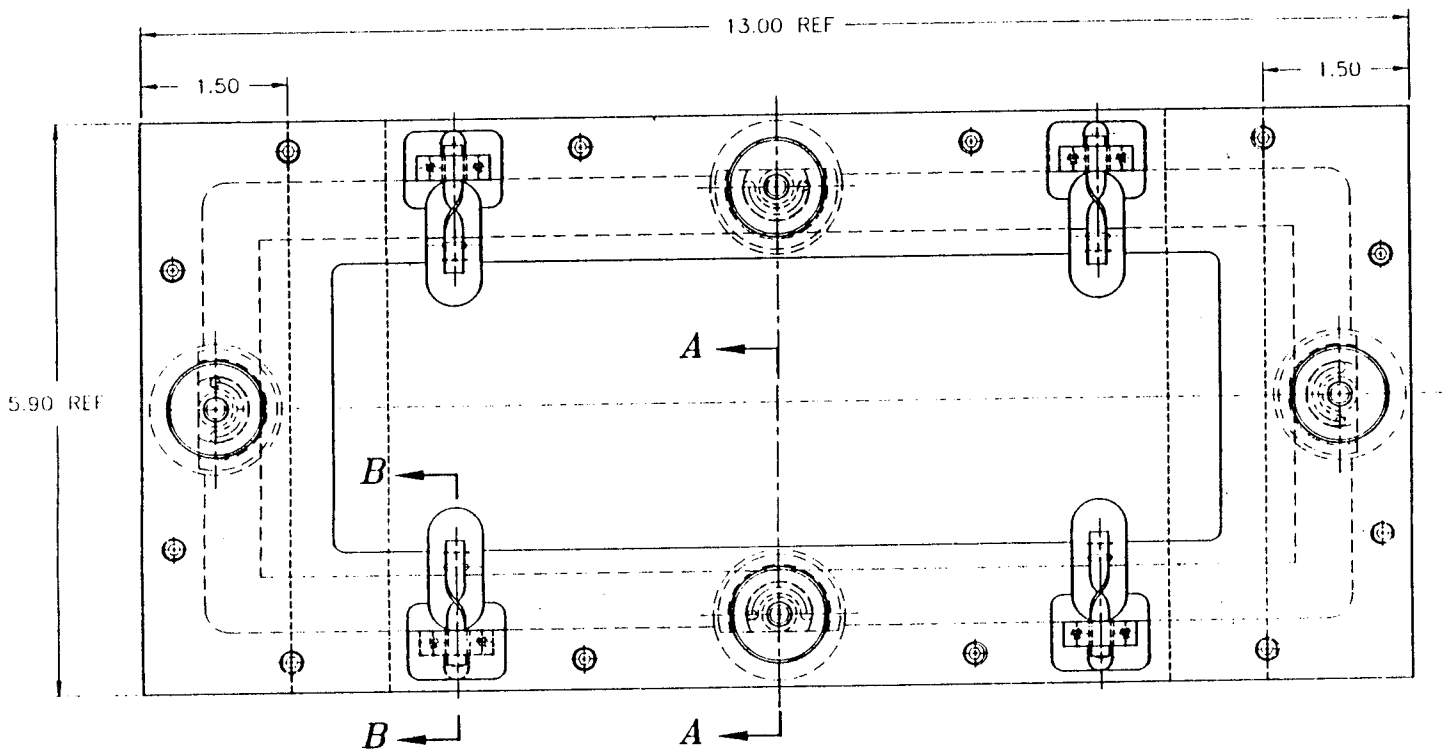

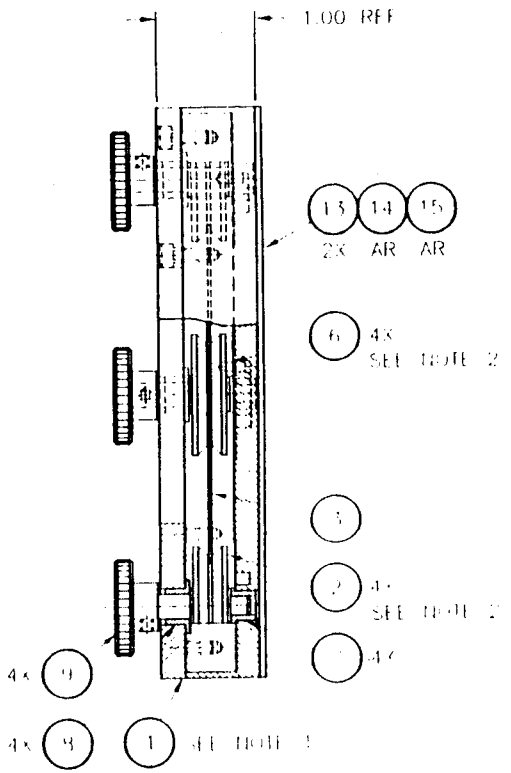

SECTION $A-A$

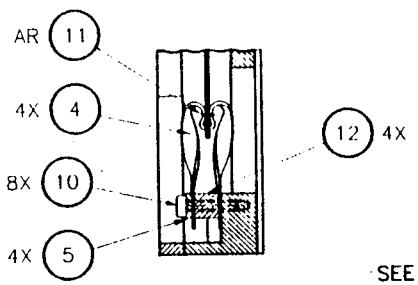

SECTION $B-B$

NOTES:

UNLESS OTHERWISE SPECIFIED

1. ITEM 1 MUST BE DISASSEMBLED TO INSTALL ITEM 2.
2. ITEM 6 (PINS) MUST BE PRESSED INTO ITEM 2 (CAGING SHAFT) BEFORE INSTALLING ITEM 2.
3. EACH LEG OF ITEM 4 (ELASTOMERIC SPRING) TO BE TWISTED 180° OPPOSITE ONE ANOTHER, AS SHOWN, PRIOR TO INSTALLING ITEM 5 (SPRING RETAINER).
4. REMOVE BURRS AND BREAK SHARP EDGES ON ALL PIECES.

SEE SEPARATE PARTS LIST

NEXT ASSY	REQ'D	USED ON
APPLICATION		

UNLESS OTHERWISE SPECIFIED DIMENSIONS ARE IN INCHES
TOLERANCES ARE:
FRACTIONS ± DECIMALS XX± ± XXX± ANGLES ± –

MATERIAL –

DO NOT SCALE DRAWING

CONTRACT NUMBER

	APPROVED	DATE
DRAWN	M. TANKENSLEY	7-10-91
CHECKED		
ENGINEER		
ENGINEER		
RELEASED		

CAMPBELL ENGINEERING
HUNTSVILLE ALABAMA

EXPERIMENT NO. 12

VIBRATION ISOLATOR ASSEMBLY

SIZE	CAGE NO	DWG NO
C	5R622	90C1706
SCALE 1/1		SHEET 1 OF 1

A.2.0 Crew Procedures

A.2.1 MCCC Crew Procedures

1. The Payload Specialist removes the experiment apparatus from storage, verifies that the power switch is off and that the mode select switch is in the "Heaters-Off" position, and places it in the glovebox. The power cable from the base is connected to the receptacle in the glovebox. The tube containing sample A (the wetting sample) is placed in the mount and the heater cables are plugged into the connectors on the base. The apparatus is positioned on edge so that one of the front CCD cameras can view the entire apparatus, paying particular attention to being able to record the digital temperature data and the top CCD camera with the macro lens will observe the marker particles..

2. The power switch is turned on. Check to see that the temperature displays are reading ambient temperature. Verify that the CCD cameras are recording the temperature readings.

3. The mode select switch is set to the "Heaters On" position. The righ-hand digital temperature display should start advancing and eventually level off at 45 C. Verify that a temperature difference of at least 10 deg. C. exists between the hot and cold end. Observe the location and configuration of the void or vapor space in the liquid. Carefully examine the interface between the liquid and the tube walls using the low power objective of the microscope. Try to ascertain if the liquid is in complete contact with the wall, or if there is a liquid-vapor-solid interface.

4. Turn on the sheet illuminator to produce a longitudinal light-cut along the axis of the sample. Verify that the CCD camera can see the configuration of the liquid and can observe the marker particles in the liquid. Try to image some the marker particles with the microscope to determine if they are moving. If motion is perceptible, darken the glovebox except for the light cut illuminator and record the motion of the marker particles with the CCD camera.

5. When observations have been completed select the "Heater Off" mode and allow the sample to cool. Remove the sample tube A and replace it with Sample Tube B (with the non-wetting sample.)

6. Repeat steps 3. and 4. above.

7.. When experiment is complete, select the "Heater Off" mode. After the sample has cooled , remove the apparatus from the glovebox and return the apparatus to storage.

A.2.2 FPM Crew Procedures

1. The Payload Specialist removes the experiment apparatus from storage and places it in the glovebox. Place the pedestal with the plain lexan surface into the clamp on the base plate. The apparatus is positioned such that one of the CCD cameras is able to observe the entire apparatus. The second CCD camera with a macro lens should be adjusted so that high resolution details of the fluid in the pulling region can be recorded. Verify that the airflow in the glovebox is off.

2. Syringe A is placed in the guide with the tip near the pedestal. A small amount of fluid is squeezed out on to the pedestal by depressing the plunger.

3. The syringe is slowly moved away from the pedestal while additional fluid is supplied by pressing the plunger. Carefully note the behavior of the fluid. If the fluid strand breaks, the pull rate should be decreased (or increased) until it becomes possible to draw a liquid strand at least a few millimeters in length. If the liquid strand doesn't break, the strand should be extended at constant pull rate, if possible, to a length of 3-5 cm and and stopped. The syringe may be clamped in place using the thumb screw. Holding this position, observe the behavior of the liquid strand. Is there any evidence of Rayleigh instability, ie. does the strand tend to ball up along its length to form a series of successive beads?

4. If there is no evidence of Rayleigh instability after a minute or so, collect the fluid back into the syringe by pulling back the plunger. Now try increasing the pull rate on successive tries with less fluid to produce thinner strands until the liquid strand breaks as it is being pulled. Verify that the CCDs are recording the procedures such that it will be possible to determine pull rate, strand diameter, and fluid breakup from post analysis of the video data. Do the thinner strands tend to breakup faster, or are they more stable?

5. After the minimum strand diameter and the time required for its breakup has been determined for the fluid in Syringe A, recover the fluid from the pedestal as much as possible using the syringe. Clean up any spills using wet wipes. Insert syringe B onto the guide and repeat the above procedure.

6. The fluids in the syringes A-F are arranged in descending order of favorable viscosity to surface tension ratio. Continue with the above procedures, determining the times for Rayleigh breakup to occur for various fiber diameters in each of the fluids supplied. Clean up any residual spills with wet wipes and remove and stow apparatus.

7. Place apparatus on the vibration isolator with the plate clamped. Insert the pedestal with the teflon disc labeled 1 into the base clamp. Using the 10 ml syringe with plain water, squeeze about 2 ml of water onto the center of the teflon disc. Carefully observe the behavior of the interface between the droplet and the disc. Try to estimate the contact angle and report such. Using the 35 mm camera, photograph the drop looking along the surface of the teflon disc as close as possible to accurately record the contact angle. When complete retract the

drop back into the syringe. Observe the oscillatory motion of the droplet caused by vibrations from the glovebox and record on video. Uncage the isolation pad and observe droplet motion to see if amplitude is damped. Record on video. If better definition of contact angle is obtained with isolator uncaged, photographs should be taken during the uncaged operation.

8. Repeat the above procedure with the other teflon discs labeled 2-6.

9. Insert the Passive Drop Positioning apparatus (PDP) in the base clamp. Using the 10 ml syringe, attempt to deploy a droplet of water in the center of the 4 teflon cones. Extrude the droplet until the water just barely misses the tips of the cones. Record the behavior of the droplet for a minute of so on video. Mechanically perturb the apparatus to test the stability of the droplet.

10. Recover all liquids and re-stow apparatus.

A.2.3 DFZ Crew Procedures

1. The Payload Specialist removes the experiment apparatus from storage and places it in the glovebox. The float pieces and alignment wires are removed from the base. The base is placed on the vibration isolator which is left caged for the initial experiments. The apparatus is positioned such that the B/W CCD camera is able to observe the entire apparatus in order to record the operation sequence. The color CCD should be have a magnified view of the liquid bridge region in order to obtain data on the frequency and amplitude of the oscillations of the system and details of the fluid behavior. Verify that the airflow in the glovebox is off.

2. Verify that the support rods have the flat ends facing each other. Adjust the support rods such that there is approximately 1 cm between them. Insert the alignment wires through the holes in the support rods. Fill the gap between the two support rods with the working fluid. Carefully withdraw the two alignment rods simultaneously. Observe the behavior of the system long enough to record the amplitude and frequency of oscillation of the system on video. Verify that the video is able to observe the motion. Verify that mission elapsed time is recorded along with this video in order to correlate with SAMS data in post-mission analysis.

3. Carefully lengthen the liquid zone by squeezing the mounting clamps to to release them and slowly pull the support rods apart a short distance. Add additional fluid as needed to keep the liquid bridge cylindrical. Some practice may be necessary to develop this procedure. After the liquid zone is approximately 2 cm long, and again at approximately 3 cm, observe the behavior of the system long enough to record the amplitude and frequency of oscillation of the system on video, both with the isolator caged and uncaged. Continue to lengthen the fluid gaps until they become unstable. Verify that that the length of the gap and the breakup of the zone was recorded on video. Readjust the spacing of the support rods to just below the critical length and reestablish the zone Now with the isolator uncaged, determine if a longer stability limit can be achieved.

4. Adjust the support rods such that there is approximately 4 cm between them. Select the short float piece with the flat ends. Insert the alignment wires through the holes in the support rods and capture the short float rod by inserting the alignment wires into two small holes in the end faces. Verify that the float rod is centered between the two support rods. Fill the gap between the float rod and the two support rods with the working fluid. Carefully withdraw the two alignment rods simultaneously, leaving the float rod suspended by the two liquid bridges. Observe the behavior of the system long enough to record the amplitude and frequency of oscillation of the system on video, as in step 2. Again verify that the video is able to observe the motion and verify that mission elapsed time is being recorded along with this video in order to correlate with SAMS data in post-mission analysis.

5. Carefully lengthen the liquid zones by squeezing the mounting clamps to to release them and slowly pull the support rods apart a short distance. Add additional fluid as needed to keep the liquid bridges cylindrical as was done in step 3. After the liquid zones are approximately 2 cm long, and again at approximately 3 cm, observe the behavior of the system long enough to record the amplitude and frequency of oscillation of the system on video, both with the isolator caged and uncaged. Continue to lengthen the fluid gaps until they become unstable. Verify that that the length of the gap and the breakup of the zone was recorded on video. Readjust the spacing of the support rods to just below the critical length and reestablish the configuration. Now with the isolator uncaged, determine if a longer stability limit can be achieved.

6. Lengthen the gap between the support rods to approximately 8 cm. Select the 6 cm end piece with the flat ends. Capture it between the support rods with the alignment wires and fill the gaps with the working fluid as before. Repeat the procedure outlined in paragraphs 4 and 5 above.

7. Reverse the support rods so that the rounded ends are facing on another with a gap of approximately 3 cm between them. Select the short float piece with rounded end and capture it with the alignment wires. Fill the gap with fluid and repeat the procedure outlined in paragraphs 4 and 5. After the stability limits have been determined, readjust the support rods to below the critical length and reestablish the liquid zones. Now add a drop or two of liquid soap or washing detergent to the zones and observe the effect. Does the liquid completely spread over the float so that the two liquid zones can exchange fluid? Does the system become unstable? Can the previous stability limits be attained? What are the new limits of stability?

8*. Adjust the gap between the support rods to approximately 8 cm and repeat the procedure described in paragraph 5 using the long float piece with rounded ends.

9. Install the sheet float zone support rods with the flat edges facing one another with a gap of approximately 1 mm between them. Insert the alignment wires so that they tough each other. Try to fill the gap with fluid If not successful, narrow the gap slightly until it becomes possible to make the fluid fill the gap. Carefully extend the gap, adding more fluid as needed until the stability limit has been reached. Verify that the gap spacing and details of the breakup have been suitably recorded.

10. Having determined the limits of stability for a single sheet float zone, move the sheet float zone support rods form a gap of approximately 5 cm. Using the alignment wires, capture the flat float plate, fill the two gaps with liquid, and determine the stability limits as before. When this has been accomplished for the pure fluid, add a drop of liquid soap as described in paragraph 7 to determine if lowering the surface tension and increasing the wetability of the solid has an effect on the stability limits.

11. As the above experiments progress, some flexibility should be maintained to allow the Payload Specialist to capitalize on what has been learned and to explore other configurations or variations that appear promising. After completion of the experiments, spilled liquids should be cleaned up using the scavenger pump and dry wipes. The apparatus is then removed from the glovebox and returned to stowage.

*If time permits. Otherwise proceed to next step.

A.3.0 Verification Tests and Computations

A.3.1 GEM 05 Battery Shorting Test

A.3.1.1 Introduction:

The GEM 05 Marangoni Convection in Closed Containers experiment uses two Archer 277-123 Temperature Modules which are panel meters that serve as combination temperature monitors and controllers. One module is used as a monitor and controller for the heater, while the other is just a monitor for the heat sink. Both are powered by a AA alkaline battery with is mounted to the rear of the meter by means of a plastic clip. Safety wires have been added to prevent the battery from accidentally becoming dislodged. No internal short circuit protection has been provided by the manufacturer. Concerns have been raised about the possibility of either an internal short circuit or the battery becoming inadvertently connected to a second voltage source inside the control box. Such an event could cause the battery to overheat and possibly rupture.

A.3.1.2 Purpose of Test:

To determine the possible consequences of an internal short in the battery operated panel meter/controllers used in the GEM 05 experiment.

A.3.1.3 Description of the Test:

The shorting test was conducted on a Radio Shack AA alkaline battery which had been in service for approximately three months. This service consisted of simply keeping the meter in a stand-by mode (typical current draw 3 μA) during this time. This approximates the history the flight battery will have experienced when the experiment is activated.

The battery terminals were shorted through a Fluke Model 77 Multimeter using the 10 Ampere tap. Initial voltage of the battery was 1.59 V before shorting. The initial discharge current was 5.5 A which dropped rapidly to approximately 5 A where it leveled off and remained for approximately 30 minutes. After this time, the current dropped rapidly to less than 1 A.

The initial temperature of the battery and the case was ambient at 24.0 °C. The battery temperature slowly rose to a maximum of 80.8 °C which was reached just as the current began dropping below 5.0 A. The maximum temperature on any exposed surfaces was 35.6 °C measured on the plastic face of the module readout. The maximum temperature reached by the cast aluminum control box was 28.3 °C on the corner near the module. All temperature measurements were made with an Omega 81 Digital Thermometer fitted with a Model 88006K Type K surface temperature probe.
The battery remained intact with no apparent swelling of other visible damage. There was no damage to the Temperature Module or to any other internal components.

In another test, a temperature module was purposely sacrificed to determine the consequences if the 12 V power supply was accidentally shorted to one of the control outputs. A Harrison power supply was connected to the controller ground and 12 V was introduced through an ammeter into each of the controller outputs. A slight initial current transient could be detected with the meter on the 1.5 amp scale after which no current flowed and the controller circuit showed open as a result of the destruction of the FET circuits. Otherwise the temperature module appeared to be unaffected except that the controller was no longer functional.

A.3.1.4 Conclusion:

A direct internal short in one of the Temperature Modules will not cause any damage to the experiment nor will it cause touch temperature (45 °C) to be exceeded on any exposed portion of the experiment. If 12 V is accidentally introduced into one of the controller outputs, the control circuit will immediately burnout in the open state and the controller cannot apply power to the heater.

A.3.1.5 Actions Taken:

The Temperature Module used as a controller has a lead that connects the positive terminal of its 1.5 V battery to a series of switches used to set the control temperature and arm the controller circuit. Even though there is no direct connection between this lead and any component that is connected to the 12 V supply, there is a potential for this lead to interact with external power sources (the 12 V. GBX Experiment power) if a wire happened to brake loose inside the unit and accidentally made contact with the 12 V experiment power. The power that could flow in this event would be limited to 2 amps by the main fuse, but in the event that this fuse did not open, considerably more heating could result in the battery than would be produced by an internal short within the temperature controller module which was measured in the tests described above. For this reason, a 1/16 A. fuse was placed in series between the negative battery terminal and ground.

The other possible path between the 12 V experiment power and the battery is through the two controller outputs that go to the bases of the switching transistors in the heater driver circuit. Other than accidental contact with a broken wire inside the unit, 12 V could be introduced to these leads if one of the switching transistors were to fail with a short between the collector and the base and and an open between the base and the emitter. The current would be limited by the 10 K load resistors between the 12 V. supply and the collector. Tests have also shown that the introduction of 12 V on either of these leads will cause an immediate open circuit in the controller that would prevent this current from reaching the battery.

Since the Temperature Module used only as a monitor has no connection to any external power or to ground, and since it has been demonstrated that and internal short cannot cause any damage or cause the touch temperature to be exceeded, it was determined that fuse protection for this module is unnecessary.

A.3.2 Calculation of Maximum Pressure in Sample Tube

Tube is initially filled with volume Vm of working fluid leaving a void of volume Vo to allow for thermal expansion. When temperature is increased from ambient, To, to To + ΔT, the volume of working fluid increases to

$$Vm(\Delta T) = Vm(1 + \beta\Delta T)$$

where β is the volumetric coefficient of expansion. The volume of the void becomes

$$Vo(\Delta T) = Vo - Vm(1 + \beta\Delta T).$$

The pressure in the tube may be written

$$P(T) = Pv(T) + Po\frac{(To + \Delta T)Vo}{To\ Vo(\Delta T)}$$

or

$$P(T) = Pv(T) + \frac{Po(1 + \Delta T/To)}{1 - \beta\Delta TVm/Vo}$$

where Pv(T) is the vapor pressure of the working fluid at temperature T.

The experiment apparatus is designed such that two heater plugs can move to accommodate any unanticipated pressure build-up which effectively increases Vo, thus reducing the pressure. Even if the heater plugs stick, the ratio of the working fluid to void (Vm/Vo) will be chosen to assure that the hoop stress in the tube, P(T) times the radius, will be at least 2.5 times lower than the rupture strength of the quartz tube for the maximum temperature that the heaters could attain in the "full-on" mode (failed heater control).

A.3.3 Overpressure Controls

Under normal operating conditions, the maximum temperature the working fluid will be exposed to will be 48 deg. C. This is well within the safe operating limits of both fluids. The fluids will be loaded with fluids at 85 deg. C., which is above the maximum temperature they would see even in the event of a failure of the control circuit and of the thermal fuse. This should provide a negative operating operating pressure under all foreseeable circumstances. In the filling procedure, a void space will be maintained equivalent to 5% volume at ambient temperature to allow for thermal expansion and to fulfill the purpose of the investigation, i.e., to understand the behavior of a melt in a partially filled container with an imposed thermal gradient.

The vapor pressure of the Krytox 148 AZ is negligible at the temperatures that could be reached by the apparatus. Even if the negative pressure is lost by ambient air slowly diffusing into the sample tube during the long storage period, the pressure of the trapped air (assuming the 5% void in the tube was now at atmospheric pressure) will be 1.088 atmospheres or 2.3 PSI overpressure at 45 deg. C. The end plugs form a tight fit but can move up to 2.5 cm within the sample tube to accommodate an overpressure. A movement of the end plug of only 0.01 cm would reduce this pressure to 1 atmosphere. For the case of H_20, the vapor pressure will increase this over pressure to 2.76 PSI and a movement of 0.024 cm would relieve this pressure.

In the event of a control failure and failure on the part of the operator to shut down the experiment when the temperature readout goes off-scale and flashes "---", the maximum temperature will be determined by the thermal fuse which will open at 72 deg. C. Again assuming the 5% void in the sample tube had reached atmospheric pressure during storage, this would result in a pressure of 1.176 atmospheres or an overpressure of 2.6 PSI being generated in the sample tube by the trapped air in the case of Krytox. A 0.022 cm movement of the end plug would relieve this pressure. In the case of H_20 the pressure would be 1.515 atmospheres or an overpressure of 7.5 PSI. A 0.1 cm movement of the end plug would be required to reduce the pressure to 1 atmosphere.

In the event of a three-fault failure (the control circuit fails in a full-on state, the operator fails to notice the flashing "---" on the readout, and the thermal fuse fails to open), the maximum temperature that can be reached with the 11.7 Watts being supplied to the heater is was found to be 80.4 deg C. Again assuming the 5% void in the sample tube had reached atmospheric pressure during storage, the trapped air in the Krytox sample would reach a maximum overpressure of 2.9 PSI which could be relieved by the end plug moving 0.025 cm. The sample tube containing H_20 will reach an overpressure of 9.9 PSI which would require a 0.15 cm movement of the end plug to drop the pressure to 1 atmosphere.

In the runaway thermal tests that were conducted, the fluids had not been loaded at elevated temperatures so there was no negative pressue in the sample tube (this would correspond to the situation if the pressure in the sample tubes had reached atmospheric during storage). Even so, the fluids were safely contained

without leakage at the pressures corresponding to the worst case temperature and pressure (80.4 deg C. and 9.9 PSI overpressure in the case of H_20). Even if the tube ruptures or if the the end plug is forced out of the sample tube, the worst that would result would be the spillage of 13 ml of hot H_20 in the glovebox.

A.3.5 Touch Temperature Test

Thermal tests were performed on the apparatus under simulated glovebox operating conditions; ambient temperature 25.3 deg. C and airflow over the cooling fins on the heatsink. Heater and heatsink temperatures were measured using the LCD panel displays. Touch temperature was measured with a type K thermocouple clamped to the outside of the sample tube near the heater plug.

The heatup and cooldown cycle is shown in the attached plot. The controller controlled the heater plug between 45.4 and 47.3 deg. C. The maximum touch temperature on the tube did not exceed 30.2 deg. C and the heat sink temperature did not exceed 28.4 deg. C.

A.4.0 Invention Disclosure

A.4.1 A Passive Vibration Isolation Device For Small Space Experiments

A.4.1.1 Introduction

The presence of a human experimenter to perform a microgravity experiment can be extremely valuable from his ability to minipulate, observe, and reconfigure if necessary. It also carries a penalty of the fact that any motion excites various vibration modes in the spacecraft that may obscure some of the effects of reduced gravity that the investigator wished to study. Similarly, mechanical devices, even some as insignificant as camera shutters, have produced measurable disturbances on rockets. Certain classes of experiments, expecially those that involve liquids in partially filled containers or in other configurations with free surfaces (such as liquid bridges, floating zones, etc.), are particularly susceptible to small periodic accelerations causes by internal forces.

A.4.1.2 Purpose Of The Invention

The purpose of this invention is to provide a simple, inexpensive device that can isolate small but sensitive experiments that are designed to be operated by the crew on a manned space vehicle from the disturbances induced by the crew's activities.

A.4.1.3 Description Of The Invention

To isolate sensitive experiments from such accelerations, a simple passive vibration isolation device has been developed. The device consists of a frame (Item 1 in Section A-A, Figure A.1.4), a caging mechanism consisting of four slotted half-discs (Item 6), an isolation plate (Item 3), and a suspension mechanism (shown in Section B-B, Figure A.1.4.).

The frame is mounted to a workbench or other suitable spacecraft structure with the isolation plate in the caged configuration. The sensitive experiment is placed on the soft steel isolation pad and held in place by means of small magnetic strips or other temporary holding means. After the experiment is readied for isolation, the four slotted half-discs are rotated until their flat portion is facing the plate and the plate is no longer constrained by the slots in the discs. After the experiment is completed, the half-discs are rotated back to the original position. The isolation plate is captured by the bevels on either side of the slot and held in the caged position by the slots.

The primary purpose of the passive vibration isolation device is to reduce as much as possible the passage of vibrations induced by human operations on board the spacecraft. The natural frequencies of the structural components in the spacecraft are typically well above 1 Hz, but the frequencies associated with human activity such as exercizing on a treadmill are typically around 3 Hz.

Therefore it is desired to make the natural frequency of the isolation device as low as practical considerations will permit, preferably well below 1 Hz. This means the suspension system must have a high compliance and be nearly critically damped.

If the sensitive experiment has a mass of 1 kg, in order to achieve a natural frequency below 1 Hz, the spring constant has to be less than 40,000 dynes/cm. This means a 40 gm force (approximately the weight of the plate) must displace the isolation plate by more than 1 cm in normal gravity.

The approach taken to provide a suitable suspension system is to use four ordinary rubber bands operating in a flex or bending mode rather than in a stretch mode. The rubber bands are arranged as shown in Section B-B of Figure 1. This arrangement has the advantage of providing a flex or bending mode for motion along each of the three axes, thus providing essentially the same degree of isolation for all directions. The doubling of each band increases the stifness by a factor of 2, but has the advantage of providing symmetrical restoring forces. Also the loop arrangment "stiffens up" at large displacements when the top or bottom of the loop encounters the walls of the frame. This provides a cushion against large transient accelerations that may occur during the mission. Finally, the bending or flexing of the rubber bands is inherently a lossey process which provides adequate damping without the need for any additional energy dissipation devices.

In the bending mode, each band has a spring constant typically on the order on 1000 dynes/cm. With four suspension points and the bands doubled, the overall spring constant will be on the order of 8000 dynes/cm. For a 1 kg suspended mass, the natural frequency will be on the order of 0.5 Hz. This is sufficiently far from the typical applied frequiencies associated with human activities to provide a reasonable degree of isolation, even with a passive system.

A.4.1.4 Advantage Over Previous Art

Several active systems have been developed to isolate space experiments from crew or vehicle disaturbances. The systems employed magnetic fields and servo loops to keep the isolated plate in the same position regardless of the motion of the external frame. By adjusting the gain of the servo loop the effective spring constant and damping factor can be varied over a wide range of values and the system can be tuned electronically in realtime to adjust to varying operating conditions. However, such devices are complex, expensive, consume power and produce waste heat. The primary advantage of the passive system presented here is a means to accomplish the same overall objective in a much simpler manner at a very small fraction of the cost. The passive device, unlike active sysems, is unconditionally stable under all operating conditions and cannot add energy to the oscillation. Perhaps the biggest advantage offer by the passive system is that it requires no power or active cooling. Therefore it is especially suited for missions in which power is limited or for applications that require operation inside temperature controlled enclosures or refrigerators where additional power dissipation would be unacceptable.